Male germ cell-associated kinase (MAK) is required for axoneme formation during ciliogenesis in zebrafish photoreceptors

Hung-Ju Chiang[1], Yuko Nishiwaki[1], Wei-Chieh Chiang[1], and Ichiro Masai[1,2]

[1]Developmental Neurobiology Unit, Okinawa Institute of Science and Technology Graduate University, Tancha, Okinawa, Japan.

[2] Correspondence should be addressed (masai@oist.jp)

Keywords: zebrafish, photoreceptor degeneration, MAK, ciliopathy, ciliogenesis

Summary statement (up to 30 words)

Male germ cell-associated kinase (MAK) is a cilium-associated serine/threonine kinase that promotes axoneme development during ciliogenesis in zebrafish photoreceptors to ensure intracellular protein transport and photoreceptor survival.

Abstract

Vertebrate photoreceptors are highly specialized retinal neurons and have cilium-derived membrane organelles called outer segments (OS), which function as platforms for phototransduction. Male germ cell-associated kinase (MAK) is a cilium-associated serine/threonine kinase, and its genetic mutation causes photoreceptor degeneration in mice and retinitis pigmentosa in humans. However, the role of MAK in photoreceptors is not fully understood. Here, we report that zebrafish *mak* mutants show rapid photoreceptor degeneration during embryonic development. In *mak* mutants, both cone and rod photoreceptors completely lack OSs and undergo apoptosis. Interestingly, zebrafish *mak* mutants fail to generate axonemes during photoreceptor ciliogenesis, whereas basal bodies and transition zones are specified. These data suggest that MAK plays a specific role in axoneme development in zebrafish, in contrast to mouse *Mak* mutants, which have elongated photoreceptor axonemes. Furthermore, the kinase activity of MAK is critical in ciliary axoneme development and photoreceptor survival. Thus, MAK is required for ciliogenesis and OS formation in zebrafish photoreceptors to ensure intracellular protein transport and photoreceptor survival.

Introduction

The vertebrate photoreceptor is highly compartmentalized to form specialized structures related to phototransduction (Fain et al., 2010). The outer segment (OS) is a specialized cilium of the photoreceptor, in which multiple photoreceptive membrane discs are regularly stacked to accommodate phototransduction molecules such as rhodopsin and opsins (Bachmann-Gagescu and Neuhauss, 2019; Chen et al., 2021). The inner segment (IS) is a mitochondria-enriched region between the OS and the nucleus. Finally, photoreceptors have a specialized synaptic structure in the most basal region, which forms the outer plexiform layer (OPL) and mediates transmission of electric signals to horizontal cells and bipolar cells (Mercer and Thoreson, 2011).

Upon photoactivation in vertebrate photoreceptors, opsins or rhodopsin absorb light energy and change their conformation, which activates Transducin, and then cGMP phosphodiesterase 6 (PDE6). PDE6 catalyzes the hydrolysis of a second messenger, cGMP. Reduction of the cGMP concentration promotes dissociation of cGMP from a cyclic nucleotide binding channel (CNG), leading to the closure of CNG, which hyperpolarizes photoreceptor membranes. All of these phototransduction molecules are specifically expressed in photoreceptors and properly transported into the OS, which is essential for photoreceptor functions (Athanasiou et al., 2018; Gulati and Palczewski, 2023; Karan et al., 2008; Wang and Deretic, 2014). Indeed, mislocalization of opsins leads to photoreceptor degeneration, although detailed mechanisms are not fully understood (Alfinito and Townes-Anderson, 2002; Lopes, 2010; Rohrer et al., 2005).

The photoreceptor OS is a highly specialized primary cilium, which consists of stacked membrane discs around a microtubule-based backbone called the axoneme (Bachmann-Gagescu and Neuhauss, 2019; Chen et al., 2021). The axoneme is anchored from the basal body in the IS of photoreceptors and extended apically through the connecting cilium. The connecting cilium bridges the IS and the OS, through which phototransduction molecules are transported from the ER, then to the Golgi and into the OS. Importantly, the connecting cilium is equivalent to the transition zone in other cell types and functions as a gating system (Park and Leroux, 2022), through which OS resident proteins are sorted and transported to

68 the OS by the intraflagellar transport (IFT) complex (Klena and Pigino, 2022) and BBSome,
69 composed of eight Bardet-Biedl syndrome (BBS) proteins (Tian et al., 2023).

70 The process of ciliary development is called ciliogenesis, which consists primarily of
71 three steps: centriole (basal body) docking to the apical plasma membrane, establishment of
72 a transition zone, and ciliary axoneme extension (Baehr et al., 2019). A number of factors
73 are indispensable for ciliogenesis. For example, CC2D2A is required by basal body
74 maturation (Gorden et al., 2008). BBS1 is required for ciliary assembly and maintenance
75 (Davis, 2007). RP1 has microtubule extension activity that promotes axoneme extension (Liu
76 et al., 2004). Because cilia work as "rail tracks" in IFT-mediated trafficking, disruption of
77 cilia affects IFT and further causes photoreceptor degeneration, suggesting that the structural
78 and functional integrity of the connecting cilium is indispensable for photoreceptor functions
79 and maintenance. Although many other factors reportedly regulate photoreceptor cilia
80 integrity (Cideciyan et al., 2007; den Hollander et al., 2006; Gao J., 2002; Gorden et al., 2008;
81 Kakakhel et al., 2020; Rao et al., 2015; Zhu et al., 2021), the underlying mechanisms are not
82 fully understood.

83 Male germ cell-associated kinase (MAK) belongs to the MAK/ICK/MOK
84 serine/threonine kinase family (Chen et al., 2013). MAK was originally identified by cross-
85 hybridization with tyrosine kinase v-ros in rat testicular cells, so it was considered to be a
86 spermatogenesis regulator (Matsushime et al., 1990). Furthermore, MAK functions as a
87 coactivator of androgen receptors (ARs) to promote AR-mediated signaling, which is
88 associated with prostate tumorigenesis (Ma et al., 2006; Wang and Kung, 2012; Xia et al.,
89 2002). In addition to the role of MAK in male reproductive organs, MAK is expressed in
90 developing rod photoreceptors (Blackshaw et al., 2004). In *Mak* knockout mice,
91 photoreceptors show abnormally elongated axonemes and malformation of membrane discs
92 in the OS, leading to photoreceptor degeneration (Omori et al., 2010). In humans, *MAK*
93 mutations cause retinitis pigmentosa (RP), in which patients progressively lose their vision
94 (Ozgul et al., 2011; Stone et al., 2011). However, human patients carrying *MAK* mutations
95 do not show elongation of the photoreceptor layer under optical coherence tomography (OCT)
96 scanning (Stone et al., 2011), which may be different from photoreceptor phenotypes of *Mak*

97 knockout mice. Thus, it is important how *mak* mutations affect ciliary regulation in
98 photoreceptors among vertebrate species.

99 In this study, we found that zebrafish photoreceptors of *mak* mutants degenerate during
100 embryonic development. In *mak* mutants, both rods and cones undergo apoptosis, although
101 their degeneration processes differ. Interestingly, *mak* mutants fail to form axonemes in
102 photoreceptor cilia, whereas basal bodies and transition zones are specified, which is the
103 opposite of mouse *Mak* knockout photoreceptors, with elongated ciliary axonemes.
104 Furthermore, both cones and rods completely lack OSs in *mak* mutants, leading to ectopic
105 distribution of opsins. MAK is essential to form axonemes and OSs in photoreceptors. Finally,
106 we confirmed that MAK kinase activity is critical for axoneme formation and photoreceptor
107 survival. Thus, MAK is essential for ciliogenesis, OS formation, and photoreceptor survival.

108 **Results**

109 ***Zebrafish pday* mutants carry a genetic mutation in *mak* gene and show photoreceptor**
110 **degeneration**

111 Zebrafish *payday* (*pday*) mutants display no visual response during the embryonic stage
112 (Muto et al., 2005). We selected *pday* homozygous mutant embryos using the optokinetic
113 response (OKR) assay and examined their phenotypes. At 6 dpf, *pday* mutants showed no
114 apparent morphological defect in body structure (Fig. 1A), but did not survive until adulthood,
115 suggesting a lethal mutation. However, under intensive feeding conditions, some mutants did
116 survive until 2 months post-fertilization (mpf), and displayed scoliosis, cardiac edema, and
117 smaller body size (Fig. 1A).

118 Next, we mapped the *pday* mutant locus with simple sequence-length polymorphism
119 (SSLP) markers (Knapik et al., 1998; Shimoda et al., 1999). The *pday* mutation was mapped
120 between two SSLP markers z23011 (1/186 miosis) and z13695 (3/186 mitosis), so the mutant
121 gene is restricted to a genomic region between 8.517 and 9.123 Mb on chromosome 24. In
122 this genomic region, 10 genes including *mak* were annotated in the zebrafish genomic
123 database (GRCz10, Ensemble release 80). Since *Mak* mutations cause photoreceptor
124 degeneration in mice (Omori et al., 2010) and humans (Ozgul et al., 2011; Stone et al., 2011),
125 we focused on the *mak* gene. First, we designed a new polymorphic marker, called Mak-N1,
126 located around 20 bp upstream of the first exon of the *mak* gene. The recombination rate of
127 Mak-N1 for *pday* mutation was 0 of 186 meiosis, suggesting that *mak* is a strong candidate
128 for the *pday* mutant gene. Next, we cloned *mak* cDNA prepared from wild-type embryos,
129 and found that *mak* cDNA consists of 15 exons (Fig. 1B) and that there are two isoforms of
130 *mak* mRNAs. One has and the other lacks exon 14 due to alternative splicing. Then, we
131 focused on the longest isoform, which has the exon 14 and it was annotated as the full-length
132 isoform on the zebrafish genomic database (mak-201, GRCz11, Ensemble release 110). We
133 amplified *mak* full-length cDNA from *pday* mutant mRNA by PCR. However, we did not
134 recover *pday* mutant full-length cDNA, but only a partial cDNA that covers the C-terminal
135 coding region from the middle of exon 7 to exon 15. Sequencing this partial cDNA fragment
136 revealed no mutation in the coding region from exons 8 to 15 in *pday* mutants. Next, we

137 amplified six DNA fragments from the *pday* mutant genome by PCR, each of which covers
138 six coding exons (exons 2 – 7). Sequencing of these fragments revealed that a non-sense
139 mutation occurs in exon 4 of the *mak* gene in *pday* mutants, which causes a premature
140 termination codon at 70R (Fig. 1B). These data suggest that the *pday* mutant gene encodes
141 MAK.

142 Next, we examined retinal phenotypes of wild-type and *pday* mutant retinas at 3,
143 4, 5, and 6 dpf (Fig. 1C, 1C'). In wild-type retinas at 3 dpf, photoreceptors differentiate to
144 form the outer nuclear layer (ONL). The OS is formed in the apical region of the ONL (Fig.
145 1C'). In *pday* mutants, the ONL was formed; however, densely labeled nuclei were observed
146 in the basal region of the ventro-central ONL (Fig. 1C, 1C'), and the OS was markedly
147 reduced (Fig. 1C'). In wild-type photoreceptors at 4 dpf, the OS was elongated. However, in
148 *pday* mutants, the ONL was decreased in thickness (Fig. 1C, 1C'), and no OS-like structure
149 was observed in the apical region (Fig. 1C'). In addition, there were pyknotic nuclei (Fig.
150 1C') and bubble-like structures (Fig. 1C, 1C'), mainly in the dorso-central ONL. In wild-
151 type embryos at 5 dpf, the ONL was divided into two subnuclear layers (Fig. 1C'), the apical
152 and basal regions of which contain nuclei of Blue/Green/Green cones and rods/UV cones,
153 respectively (D'Orazi et al., 2020; Oel et al., 2020). However, in *pday* mutants, the dorso-
154 central ONL drastically decreased in thickness (Fig. 1C) and contained flattened nuclei (Fig.
155 1C, 1C'). In wild-type embryos at 6 dpf, photoreceptors showed more mature shapes in the
156 ONL. However, in *pday* mutants, most photoreceptor nuclei disappeared in the dorso-central
157 retina (Fig. 1C), so there are very flat nuclei in the outermost region of the retina, which are
158 difficult to define as the ONL or horizontal cells (Fig. 1C'). Interestingly, in *pday* mutants,
159 ONL thickness was less affected in the retinal region more ventral to the optic nerve head,
160 even at 6 dpf (Fig. 1C), although the OS is absent and bubble-like structures are occasionally
161 observed (Fig. 1C). Thus, the sensitivity of photoreceptor degeneration differs between the
162 dorso-central region and the ventral region of the neural retina. In addition, other retinal
163 layers, namely the inner nuclear layer (INL), the inner plexiform layer (IPL), and the retinal
164 ganglion cell layer (RGCL) seemed to be intact in *pday* mutants from 3 to 6 dpf (Fig. 1C),
165 suggesting photoreceptor-specific degeneration in *pday* mutants.

166 To confirm photoreceptor degeneration in mutant retinas at 6pf, we introduced a
167 transgenic line *Tg[crx:eGFP]*, which expresses eGFP in photoreceptor precursors and
168 mature rod and cone photoreceptors under control of the *cone-rod homeobox* (*crx*) promoter
169 (Suzuki et al., 2013) (Fig. 1D). In wild-type retinas, eGFP signals were detected in the ONL
170 at 6 dpf. However, in *pday* mutant retinas, eGFP signals disappeared in the dorso-central
171 retina at 6 dpf (Fig. 1D). Measurements of the thickness of eGFP-positive areas revealed that
172 photoreceptor degeneration is more severe in the dorso-central retina than in the ventral retina
173 at 6 dpf (Fig. 1E). Thus, photoreceptors undergo degeneration in *pday* mutants.
174
175 **Both rods and cones degenerate in *pday* mutants**
176 In human *MAK*-associated RP patients, rods degenerate more prominently (Ozgul et al., 2011;
177 Stone et al., 2011). To evaluate rod and cone degeneration separately, we generated double
178 transgenic lines, *Tg[rho:NLS-eGFP; gnat2:NLS-tdTomato*], to visualize rods and cones with
179 eGFP and tdTomato fluorescence, respectively, and introduced them into *pday* mutants (Fig.
180 2-S1A). In wild-type retinas, eGFP expression in rods was strong and dense in the ventral
181 ONL but relatively weak and sparse in the dorso-central ONL at 3 dpf (Fig. S1A). On the
182 other hand, eGFP expression was very faint in *pday* mutant retinas under the same conditions.
183 However, when the laser intensity was increased, eGFP expression was detected (Fig. S1A),
184 suggesting that rods are maintained in 3 dpf *pday* mutant retinas, although the rhodopsin
185 promoter does not effectively drive *eGFP* mRNA or else translation of *eGFP* mRNA to eGFP
186 protein was affected in *pday* mutants. Therefore, in later experiments using *Tg[rho:NLS-*
187 *eGFP]*, we applied higher laser intensity to *pday* mutant scanning, and compared rod
188 phenotypes between *pday* mutants and their wild-type siblings.
189 Since photoreceptor degeneration is more severe in the dorso-central retina,
190 compared with the ventral retina at 6 dpf (Fig. 1D, 1E), we visualized morphology of rods
191 and cones using *Tg[rho:NLS-eGFP; gnat2:NLS-tdTomato*] at 3, 4, 5, and 6 dpf (Fig. 2A, 2B),
192 and focused on the dorsal and ventral ONL regions (Fig. 2C-F). First, we examined rods (Fig.
193 2A). In wild-type retinas at 3 dpf, rods were sparse in the dorsal ONL (Fig. 2C), but densely
194 produced in the ventral ONL (Fig. 2D). In *pday* mutants, many rods show very round nuclei

195 in both the dorsal and ventral ONL (Fig. 2C and 2D). Interestingly, eGFP signals were
196 predominantly localized in nuclei of wild-type rods because eGFP was tagged with a nuclear
197 localization sequence (NLS); however, eGFP signals were often excluded from the round
198 nuclei of *pday* mutant rods, suggesting apoptotic-like pyknotic nuclei of *pday* mutant rods.
199 After 4 dpf, in wild-type retinas, rods progressively increased in number and aligned along
200 the dorsal ONL. Their nuclei are positioned in the most basal region of the ONL, and rods
201 extend a process to form the OS in the apical region of the ONL (Fig. 2C). On the other hand,
202 rods are more densely differentiated in the ventral ONL (Fig. 2D). However, in *pday* mutants
203 at 4 dpf, rods almost disappeared in both the dorsal and ventral ONL. Only a few rods were
204 retained, but displayed pyknotic nuclei or were excluded from the ONL (Fig. 2C and 2D). In
205 *pday* mutants at 5 and 6 dpf, rods disappeared in most regions of the ONL (Fig. 2C and 2D),
206 except in the peripheral retina adjacent to the ciliary marginal zone (CMZ) where new
207 photoreceptors continued to be produced by retinal stem cells. So, rods are eliminated soon
208 after they are specified from the CMZ. To understand the spatio-temporal pattern of rod
209 degeneration, we counted the number of rod nuclei along the DV axis of the retina (Fig. S1B).
210 The number of rods progressively decreased in the central ONL of *pday* mutant retinas and
211 were completely eliminated, except in the peripheral region near the CMZ area at 5 and 6
212 dpf.

213 Next, we examined cones at 3, 4, 5 and 6 dpf (Fig. 2B). In wild-type retinas at 3
214 dpf, cones differentiated uniformly in the dorsal ONL (Fig. 2E); however, cone density
215 became progressively more sparse toward the CMZ region in the ventral ONL (Fig. 2F), a
216 pattern complimentary to that of rods (Fig. 2D). In *pday* mutant retinas, cones normally
217 differentiated to form a spatial pattern similar to that of wild-type retinas (Fig. 2E, 2F).
218 However, there were tdTomato-negative rounded nuclei in both the dorsal and ventral ONL
219 (Fig. 2E and 2F), whose positions are identical to pyknotic-like rod nuclei (Fig. 2C and 2D).
220 These data confirm that rods abnormally invaded the cone cell layer in *pday* mutants at 3 dpf.
221 After 4 dpf, in wild-type retinas, cones form two subnuclear layers in the dorso-central ONL
222 (Fig. 2E). However, cone density was complimentary to rod density and became
223 progressively more sparse toward the CMZ region in the ventral ONL (Fig. 2F). In *pday*

224 mutants at 4 dpf, segregation of two cone subnuclear layers was incomplete in the dorso-
225 central ONL (Fig. 2E). Furthermore, cones were sparse and shortened in the ventral ONL
226 (Fig. 2F). In *pday* mutants at 5 dpf, cones were shortened in the dorsal ONL (Fig. 2E).
227 Interestingly, cone density was increased toward the CMZ in the ventral ONL of *pday*
228 mutants (Fig. 2F), where rods failed to be maintained (Fig. 2D). In *pday* mutants at 6 dpf,
229 cones were extremely fattened and there were gaps between them in the dorsal ONL (Fig.
230 2E), indicating that cones are eliminated. Furthermore, cones were similarly flattened in the
231 ventro-central ONL (Fig. 2F), whereas cones were uniformly produced and less flattened
232 toward the CMZ of the ventral ONL (Fig. 2F). Therefore, in *pday* mutants, a substantial
233 fraction of cones was retained in the central retina at 5 dpf, even though their shape became
234 flattened. In *pday* mutants at 6 dpf, cones eventually disappeared, especially in the dorso-
235 central ONL.
236 Taken together, these data suggest that rods undergo acute apoptosis-like cell death
237 in *pday* mutants from 3 to 4 dpf (Fig. 2G). On the other hand, cones undergo progressive
238 shrinkage after 4 dpf and eventually disappear by 6 dpf in *pday* mutants (Fig. 2G), although
239 cone degeneration is less severe in the peripheral region of the ventral ONL.
240
241 **Both rods and cones undergo apoptosis in *pday* mutants**
242 Condensed rod nuclei in *pday* mutants at 3dpf (Fig. 2C, 2D) are reminiscent of apoptosis, in
243 which chromatin condensation is a hallmark (Oberhammer et al., 1994). We performed TdT-
244 mediated dUTP-nick-end labeling (TUNEL) to *pday* mutant retinas at 3, 4, and 5 dpf (Fig.
245 3A, 3A', Fig. S2A). In wild-type retinas, the number of TUNEL-positive cells was
246 continuously very low in the ONL (Fig. 3A, Fig. S2A). In *pday* mutant retinas at 3 dpf,
247 TUNEL signals were detected prominently in the central and ventral ONL (Fig. 3A'), which
248 is consistent with our observation that rod pyknotic nuclei were detected at 3 dpf (Fig. 2C,
249 2D), suggesting that these early TUNEL-positive cells are likely to be rods. In *pday* mutant
250 retinas at 4 dpf, TUNEL signals increased prominently in the dorsal and central ONL (Fig.
251 3A'). In *pday* mutant retinas at 5 dpf, TUNEL signals were detected prominently in the dorsal
252 and central ONL (Fig. 3A'). Interestingly, TUNEL-positive cells were positioned in a very

253 thin central ONL of 5 dpf *pday* mutant retinas (Fig. 3A'), suggesting that these late TUNEL-
254 positive cells are likely to be cones. Number of TUNEL-positive cells was higher in *pday*
255 mutant ONL than wild-type ONL at 3 dpf, but the difference was not significant. However,
256 the number of TUNEL-positive cells was the highest in *pday* mutant ONL at 4 dpf and was
257 still significantly higher in *pday* mutant ONL at 5 dpf, compared with wild-type ONL (Fig.
258 S2A).

259 Next, we examined whether cones undergo apoptosis in *pday* mutants. First, we
260 carried out double labeling of 5-dpf, wild-type and *pday* mutant retinas with anti-zebrafish
261 rhodopsin (Vihtelic et al., 1999) and zpr1 (Larison and Bremiller, 1990) antibodies, which
262 label rod OSs and double-cone-type photoreceptors (red/green cones), respectively (Fig. 3B).
263 Consistent with data of *Tg[rho:NLS-eGFP; gnat2:NLS-tdTomato]* (Fig. 2), rods were only
264 detected in the peripheral region of the dorsal and ventral ONL (Fig. 3B'). On the other hand,
265 cones were observed in the peripheral region of the dorsal and ventral ONL and as very
266 flattened cells in the central ONL (Fig. 3B'). Next, we carried out TUNEL of 5-dpf, wild-
267 type and *pday* mutant retinas combined with zpr1 antibody labeling (Fig. 3C). Many TUNEL-
268 positive cells were observed in dorsal, central and ventral ONL (Fig. 3C'). A significant
269 fraction of these TUNEL-positive cells was associated with zpr1 signals (Fig. 3C'). Third,
270 we carried out TUNEL in 5-dpf, wild-type and *pday* mutant retinas combined with anti-
271 rhodopsin antibody labeling (Fig. 3D). Many TUNEL-positive cells were observed in dorsal,
272 central and ventral ONL (Fig. 3D'). However, rhodopsin signals were detected only in the
273 CMZ of dorsal and ventral ONL (Fig. 3D'), but not in the central ONL. Many TUNEL signals
274 were not associated with rhodopsin signals in the central ONL (Fig. 3D'). Consistent with
275 our observation that almost all flattened photoreceptors in the central ONL at 5 dpf are cones
276 (Fig. 2), these data suggest that flattened cones undergo apoptosis at or before 5 dpf. TUNEL
277 analysis also revealed that the number of TUNEL signals in other retinal layers, INL, and
278 RGCL, was not significantly different between *pday* mutants and wild-type siblings at stages
279 3, 4, or 5 dpf (Fig. S2B, S2C), although TUNEL number in the INL was higher in *pday*
280 mutants than in wild-type siblings at 4 dpf (Fig. S2B), suggesting that apoptosis is specific
281 to photoreceptors.

282 To confirm that both rods and cones undergo apoptosis in *pday* mutants, we
283 combined a transgenic line *Tg[hsp:mCherry-Bcl2]*, which expresses an anti-apoptotic protein
284 Bcl2 (Nishiwaki and Masai, 2020), with *pday* mutants and evaluated cell survival by labeling
285 with zpr1 (Larison and Bremiller, 1990) and zpr3 (Gao et al., 2022) antibodies, which
286 visualize double cone photoreceptors and rhodopsin/green opsin, respectively. Bcl2
287 overexpression significantly rescued survival of both cones and rods in *pday* mutants at 6 dpf
288 (Fig. 3E, 3F; Fig. S2D, S2E) even along the DV axis (Fig. S2F), suggesting that both cones
289 and rods undergo apoptosis in *pday* mutants.
290 Although rods and cones survived in *pday* mutants that overexpressed Bcl2, zpr3
291 signals fail to be localized in the OS, but spread in the plasma membrane throughout the cell
292 body, including the basal synaptic region (Fig. 3F'), suggesting that green opsin and
293 rhodopsin are mislocalized in Bcl2-overexpressing *pday* mutant photoreceptors. Furthermore,
294 photoreceptor nuclear shape was different between Bcl2-overexpressing *pday* mutants and
295 wild-type siblings (Fig. S2G). In addition, Bcl2 overexpression did not restore OKR of *pday*
296 mutants (Fig. S2H). These data suggest that MAK activity is primarily required for visual
297 functions of photoreceptors, disruption of which may subsequently cause Bax-mediated
298 apoptosis.
299
300 ***mak* is responsible for *pday* mutant phenotypes**
301 To validate whether the *mak* gene is responsible for *pday* mutant phenotypes, we generated
302 a zebrafish transgenic line *Tg[crx:eGFP-MAK],* which expresses the N-terminal eGFP-
303 tagged, full-length isoform of MAK under control of the *crx* promotor. A transgenic line
304 *Tg[crx:eGFP]* was used as a control. Labeling with zpr1 antibody revealed that
305 *Tg[crx:eGFP-MAK]* rescued cone photoreceptor degeneration in *pday* mutants at 6 dpf,
306 whereas *Tg[crx:eGFP]* did not (Fig. 4A, 4A', and 4B). Furthermore, *Tg[crx:eGFP-MAK]*
307 restored the visual activity of *pday* mutants at 6 dpf, whereas *Tg[crx:eGFP]* did not (Fig.
308 4C). Thus, *mak* is responsible for *pday* mutant phenotypes: photoreceptor degeneration, and
309 visual response defects.
310

311 **MAK is localized in the connecting cilium and promotes axoneme development during**
312 **ciliogenesis**

313 To examine the spatio-temporal profile of *mak* mRNA expression during embryonic
314 development, we performed whole-mount *in situ* hybridization of zebrafish embryos from
315 the 1-cell stage to 72 hpf (Fig. 5A). *mak* mRNA is ubiquitously expressed from 1- to 4-cell
316 stages, indicating maternal mRNA expression. *mak* mRNA expression disappeared at the
317 50%-epiboly stage, but was detected in Kupffer's vesicle, a ciliated embryonic organ that is
318 important for left-right asymmetry patterning (Essner et al., 2005), at the tail-bud stage. At
319 24 hpf, *mak* mRNA is ubiquitously expressed in the central nervous system, and especially
320 strongly expressed in the epiphysis and retina. At 48 hpf, *mak* mRNA is prominently
321 expressed in the brain, the retina, and the pectoral fin bud. At 72 hpf, *mak* mRNA is highly
322 expressed in the brain, including the optic tectum and the photoreceptor layer of the retina.
323 Thus, *mak* mRNA is expressed in various cell types in zebrafish embryos, including
324 Kupffer's vesicle and retinal and pineal photoreceptors, in which ciliation plays a key role in
325 supporting these cell functions (Essner et al., 2005; Liu et al., 2004; Sukumaran and Perkins,
326 2009; Zhai et al., 2014). In addition, zebrafish mutants with cilia defects tend to develop
327 scoliosis (Gray et al., 2021; Latour et al., 2020; Wang et al., 2022), which was observed in
328 *pday* mutants at 2 mpf (Fig. 1A). Thus, Mak regulates cilium-associated mechanisms in the
329 photoreceptors in zebrafish.

330 Next, we examined MAK protein localization in zebrafish photoreceptors by tracking
331 the eGFP signal in *Tg[crx:eGFP-MAK]* retinas. eGFP-MAK is localized in a stem-like
332 structure inside the OS of live photoreceptors (Fig. 5B). Next, we examined double labeling
333 of *Tg[crx:eGFP-MAK]* retinas with anti-GFP antibody and anti-acetylated α-tubulin
334 antibody. The latter mainly labels the ciliary axoneme. eGFP-MAK was co-localized to the
335 ciliary axoneme visualized by an anti-acetylated α-tubulin antibody (Fig. 5C, Fig. S3). Thus,
336 MAK is a ciliary protein in photoreceptors.

337 Next, to examine the ciliary structure in *pday* mutant photoreceptors, we used anti-
338 γ tubulin, anti-Eyes Shut homolog (EYS), and anti-acetylated α tubulin antibodies, which
339 visualize the basal body, the transition zone, and the axoneme of the cilium, respectively

340 (Malicki and Johnson, 2017; Messchaert et al., 2018). Double labeling of 3-dpf, wild-type
341 and *pday* mutant retinas with anti-acetylated α tubulin and anti-EYS antibodies revealed that
342 EYS signals were normally detected, but acetylated α tubulin signals were absent in *pday*
343 mutant photoreceptors (Fig. 6A). Next, double labeling of 3-dpf, wild-type and *pday* mutant
344 retinas with anti-γ tubulin and anti-EYS antibodies revealed that both γ tubulin and EYS
345 signals were normally associated in *pday* mutant photoreceptors (Fig. 6B). These data
346 indicate that the ciliary axoneme is absent in 3-dpf *pday* mutant photoreceptors, whereas the
347 basal body and the transition zone seem to be normal, suggesting that the ciliary axoneme is
348 the primary target of MAK.

349 The OS is considered to be a specialized cilium of photoreceptors (Bachmann-Gagescu
350 and Neuhauss, 2019; Chen et al., 2021). Arl13b is a Joubert syndrome protein, which is
351 localized in the primary cilium and mutated in zebrafish *scorpion* (*sco*) mutants (Duldulao et
352 al., 2009). In addition, GFP-tagged Arl13b visualizes cilia in zebrafish (Bachmann-Gagescu
353 et al., 2011; Borovina et al., 2010). We established two zebrafish transgenic lines,
354 *Tg[gnat2:arl13b-tdTomato; rho:arl13b-eGFP]*, which visualize the OSs of cones and rods,
355 respectively, in wild-type retinas (Fig. 6C). However, both Arl13b-tdTomato and Arl13b-
356 GFP expression were absent in 3-dpf *pday* mutant photoreceptors, suggesting that the OS
357 fails to be formed in both cones and rods of *pday* mutants. Thus, OS formation is
358 compromised in *pday* mutant photoreceptors, which may result from the absence of the
359 ciliary axoneme.

360 To confirm ciliary phenotypes in *pday* mutant photoreceptors, we applied electron
361 microscopy (EM) to examine the ultrastructure of wild-type and *pday* mutant photoreceptors
362 at 3 dpf (Fig. 6D, 6E). In wild-type photoreceptors at 3 dpf, photoreceptors show columnar
363 shapes and their OSs started to form (Fig. 6D). On the other hand, OSs were not observed in
364 *pday* mutant photoreceptors (Fig. 6E). Higher magnification EM images detected a basal
365 body, which is a pair of centrioles near the apical domain underneath the OS, as well as a
366 long extension from the basal body, which corresponds to the transition zone and the
367 axoneme, in wild-type photoreceptors (Fig. 6D'). However, a basal body and only a short
368 extension from the basal body, which is likely to correspond to only the transition zone, were

369 observed in *pday* mutant photoreceptors (Fig. 6E'). Taken together, these data suggest that
370 the OS and the ciliary axoneme are absent in *pday* mutant photoreceptors, whereas the basal
371 body and transition zone are normally formed. Thus, MAK regulates photoreceptor
372 ciliogenesis by promoting axonemal formation.
373

374 **Phototransduction molecules fail to be transported to the OS in *pday* mutant**
375 **photoreceptors**

376 Phototransduction molecules such as rhodopsin and opsins are transported to the OS through
377 the cilium (Bachmann-Gagescu and Neuhauss, 2019; Chen et al., 2021). Therefore, we
378 examined distributions of opsins and rhodopsin in *pday* mutant photoreceptors using zpr3
379 (Gao et al., 2022) and 1D4 (Yin et al., 2012) antibodies, which label green opsin/rhodopsin
380 and red opsin in zebrafish, respectively. In 3 dpf wild-type photoreceptors, green
381 opsin/rhodopsin and red opsin were normally localized in the OS (Fig. 6F, 6G). However, in
382 *pday* mutants, these opsins were mislocalized to the IS, plasma membrane, and the basal
383 synaptic region (Fig. 6F, 6G). It is likely that OS formation defects cause the failure in
384 transport of phototransduction molecules to the OS in zebrafish *mak* mutants.
385

386 **Kinase activity of MAK is essential for photoreceptor survival and ciliary axoneme**
387 **formation**

388 To understand how MAK regulates photoreceptor survival and ciliary axoneme formation,
389 we focused on kinase-associated motifs (Wang and Kung, 2012) of MAK and conducted site-
390 directed mutagenesis to silence kinase activity (Fig. 7A). Like human and mouse MAK, the
391 kinase domain is located at the N-terminal region of zebrafish MAK, which covers amino
392 acids 4 to 285 of the 633-aa full-length protein (Fig. S4). It was reported that KR (32-33 aa)
393 and TDY (157-159 aa) are required for kinase activity as an ATP-binding motif and an
394 autophosphorylation site, respectively (Wang and Kung, 2012). We designed two kinase-
395 dead mutants of zebrafish MAK, namely AR MAK and ADF MAK, by replacing KR and
396 TDY in wild-type zebrafish MAK with AR and ADF, respectively (Fig. 7A). We also
397 prepared DM MAK, which carries both AR and ADF mutant motifs. *In vitro* kinase assay

398 using MAK proteins purified from an *E.* coli. expression system revealed that all three
399 kinase-dead MAK mutants, AR MAK, ADF MAK, and DM MAK, failed to phosphorylate
400 a MAK mock substrate, myelin basic protein (MBP), indicating that MAK kinase activity is
401 silenced in either mutant, AR MAK, ADF MAK, or DM MAK (Fig. 7B).

402 Next, we generated zebrafish transgenic lines, *Tg[crx:eGFP-AR MAK]*,
403 *Tg[crx:eGFP-ADF MAK]*, and *Tg[crx:eGFP-DM MAK]*, by introducing kinase-dead mutant
404 motifs into the wild-type MAK-expressing construct, *Tg[crx:eGFP-WT MAK]*. First, we
405 examined subcellular localization of these three kinase-dead mutant MAK proteins in
406 zebrafish photoreceptors by labeling these transgenic wild-type retinas with anti-GFP
407 antibody (Fig. 7C). eGFP-WT MAK was localized in a stem-like pattern similar to the
408 axoneme of photoreceptor cilium. However, eGFP-AR MAK was localized in a spot-like
409 region near the proximal region of photoreceptor cilium, which seems to correspond to either
410 the basal body or the transition zone. Thus, ATP-binding activity is important for proper
411 localization of MAK in the axoneme of photoreceptor cilium. eGFP-ADF MAK was likely
412 to be localized in the axoneme of photoreceptor cilium, but its expression level was low,
413 suggesting that GFP-ADF MAK may be unstable. GFP-DM MAK showed a low expression
414 level as well, which made it difficult to define its subcellular localization. These data suggest
415 that MAK kinase activity influences its localization in the axoneme of photoreceptor cilium.

416 Next, using zpr1 antibody, we examined whether MAK kinase activity is required for
417 survival of double-cone photoreceptors. We combined transgenic lines, *Tg[crx:eGFP-AR*
418 *MAK]*, *Tg[crx:eGFP-ADF MAK]*, and *Tg[crx:eGFP-DM MAK]*, with the *pday* mutants. In
419 contrast to *Tg[crx:eGFP-WT MAK]*, all three kinase-dead mutant MAK transgenes fail to
420 rescue survival of double-cone photoreceptors in the dorso-central ONL at 6 dpf (Fig. 7D),
421 suggesting that MAK kinase activity is important for photoreceptor survival.

422 To determine whether MAK kinase activity is required for ciliary axoneme formation,
423 we examined ciliary axonemes in *pday* mutants by labeling *pday* mutants combined with
424 *Tg[crx:eGFP-AR MAK]*, *Tg[crx:eGFP-ADF MAK]*, and *Tg[crx:eGFP-DM MAK]* with anti-
425 acetylated α tubulin antibody. In contrast to *Tg[crx:eGFP-WT MAK]*, all three kinase-dead
426 mutant MAK transgenes failed to rescue axoneme formation at 6 dpf (Fig. 7E). Thus, MAK

427 kinase activity is critical for ciliary axoneme development and photoreceptor survival (Fig.
428 8).

429 **Discussion**

430 In this study, we showed that zebrafish *mak* mutants show progressive degeneration of
431 photoreceptors during embryonic development. In *mak* mutants, both rods and cones undergo
432 apoptosis; however, in contrast to rods, cones do not display an acute apoptotic phenotype
433 such as condensed nuclei, but rather a progressive shrinkage of cell volume. In *mak* mutants,
434 photoreceptor cilia completely lack axonemes, whereas basal bodies and transition zones
435 seem to be specified. Since a photoreceptor cilium is essential for IFT-mediated protein
436 transport to the OS, it is likely that IFT-mediated ciliary transport is affected in *mak* mutants.
437 Consistently, the OS is absent in *mak* mutants. OS resident proteins, rhodopsin and opsins,
438 are abnormally distributed in photoreceptors. Finally, we confirmed that the kinase activity
439 of MAK is essential for axoneme formation and photoreceptor maintenance. Thus, MAK is
440 essential for photoreceptor ciliogenesis, especially axoneme formation, in zebrafish.

441 In zebrafish, photoreceptor precursors undergo one round of asymmetric cell division
442 to produce two daughter cones after 60 hpf, in which apically localized centrosomes start
443 ciliogenesis (Zolessi et al., 2021). The primary cilium is generated by either extracellular or
444 intracellular pathways in vertebrate photoreceptors (Breslow and Holland, 2019). In either
445 case, the first step of ciliogenesis is the removal of CP110 from a distal appendage of the
446 mother centriole, which enables ARL13b and components of IFT-A and IFT-B to assemble
447 at the apical surface of a distal appendage of the mother centriole in a rab8-dependent manner
448 (Breslow and Holland, 2019; Ge et al., 2022). The second step is formation of the transition
449 zone by the transport of MKS and NPHP module components (Park and Leroux, 2022). The
450 third step is extension of the axoneme through IFT-mediated ciliary transport, which
451 transports and adds α-/β-tubulin dimers to the plus end of the microtubule comprising the
452 axoneme (Brouhard and Rice, 2018; Ge et al., 2022; Nakayama and Katoh, 2018).

453 In humans and other animal models, including zebrafish and mice, many genetic
454 mutations showing defects in photoreceptor ciliogenesis have been identified (Chen et al.,
455 2021). In zebrafish mutants of transition zone components, which are classified into three
456 modules, MKS, NPHP, and core holding module, the gating mechanism of the transition
457 zone, which selectively transports phototransduction molecules such as opsins into the OS,

458 is compromised, resulting in ectopic distribution of these OS-resident proteins outside the
459 OS (Wang et al., 2022). However, the axoneme itself is formed in almost all of these
460 transition-zone-defective mutants (Wang et al., 2022). In zebrafish mutants of BBS
461 components, which cooperate with IFT to regulate intra-ciliary transport (Tian et al., 2023),
462 OS non-resident proteins are mislocalized into the OS, but axoneme and the OS are formed
463 (Masek et al., 2022). Furthermore, in zebrafish *arl13b* mutants, with compromised cargo
464 release in the OS, the axoneme and the OS are reduced in size, but still formed (Song et al.,
465 2016). Thus, most ciliogenesis-defective mutants show formation of axoneme structure in
466 photoreceptors. However, there are a few exceptions. In zebrafish mutants of an IFT-B
467 component, IFT88 (also named *oval*), Traf3ip1 (also named *elipsa*), and a Kinesin II family
468 protein Kif3a, the axoneme and the OS are totally absent in photoreceptors (Krock and
469 Perkins, 2008; Omori et al., 2008; Sukumaran and Perkins, 2009; Zhu et al., 2021).
470 Interestingly, in IFT88 (*oval*) and Traf3ip1 (*elipsa*) mutants, a single spot-like γ-tubulin or
471 centrin signal is detected in the apical region of photoreceptors, similar to zebrafish *mak*
472 mutants, suggesting that basal bodies are formed in both mutants (Omori et al., 2008;
473 Sukumaran and Perkins, 2009; Tsujikawa and Malicki, 2004). Thus, it is likely that MAK
474 cooperates with anterograde IFT complexes including IFT88 to promote axoneme formation
475 during ciliogenesis.

476 In this study, we show that overexpression of wild-type MAK, using the
477 photoreceptor-specific *crx* promoter recovers formation of axonemes, leading to survival of
478 functional photoreceptors, in *mak* mutants. However, overexpression of kinase-mutant forms
479 of MAK, AR MAK and ADF MAK, which disrupt the ATP-binding motif of the kinase
480 domain and autophosphorylation sites, fail to rescue defects in axoneme and cell survival, so
481 phosphorylation events on MAK kinase substrates are necessary for axoneme formation.
482 Interestingly, GFP-tagged AR MAK is localized in a single spot area near the apical region
483 of photoreceptors, which seems to correspond to the basal body or transition zone, whereas
484 GFP-tagged, wild-type MAK is located along the proximo-distal axis of the axoneme. One
485 possibility is that a target protein or proteins of MAK-mediated phosphorylation exist near
486 the basal body or transition zone, and that these target proteins move with MAK along the

487 axoneme after their phosphorylation by MAK. Another possibility is that MAK interacts with
488 adaptor proteins that are localized in the basal body or transition zone to support MAK
489 substrate phosphorylation for ciliogenesis. At present, a molecular network of MAK
490 phosphorylation substrates and adaptor proteins that facilitate MAK substrate
491 phosphorylation is unknown in zebrafish; however, since the IFT complex is assembled and
492 transported through the transition zone in the first step of ciliogenesis (Breslow and Holland,
493 2019), IFT complex components may be promising candidates to promote MAK substrate
494 phosphorylation.

495 MAK genes share a highly conserved amino acid sequence between zebrafish and
496 humans (51.38 % amino acid identity), especially the N-terminal kinase domain (88.65 %
497 amino acid identity). However, in contrast to zebrafish *mak* mutants, the axoneme is not
498 shortened, but is elongated in mouse *Mak* mutants (Omori et al., 2010). It is an interesting
499 question why *mak* gene knockout induces such opposite phonotypes in zebrafish and mice.
500 From a phylogenetic point of view, MAK belongs to the MAK/ICK/MOK serine/threonine
501 kinase family, all members of which share a highly conserved kinase domain (Chen et al.,
502 2013; Miyata and Nishida, 1999). CILK1 (previously known as ICK) is a member of this
503 kinase family and is now classified as a paralog of MAK. Indeed, human CILK1 shows a
504 highly similar amino acid sequence in the kinase domain to that of zebrafish MAK (81.5%
505 amino acid identity). Interestingly, in *Cilk1* mouse mutants, the photoreceptor ciliary
506 axoneme is shortened compared with that of wild-type controls (Chaya et al., 2014).
507 Furthermore, mouse CILK1 interacts with IFT-B components, including IFT88 (Nakamura
508 et al., 2020). Since a CILK1 homologous gene has not been identified in the zebrafish
509 genomic database, zebrafish MAK and mouse CILK1 may share a common regulatory
510 pathway for axoneme formation during ciliogenesis. In the future, it will be important to
511 investigate whether zebrafish MAK cooperates with IFT-B to regulate axoneme formation
512 during ciliogenesis.

513 Another interesting finding is that there is a difference in degeneration of rods and
514 cones in *mak* mutants. In *mak* mutants, the ONL progressively degenerates from 3 dpf and
515 disappears by 6 dpf. Using zebrafish transgenic lines, which visualize rods and cones

516 separately, we found that rods frequently show pyknotic nuclei, which are commonly
517 observed in apoptosis, at 3 dpf in *mak* mutants, and that the number of rods is markedly
518 decreased at 4 dpf. Since TUNEL signals increase to a maximum at 4 dpf and then decrease
519 in *mak* mutant ONL, it is likely that most TUNEL-positive photoreceptors at 3 and 4 dpf in
520 *mak* mutants are rods. On the other hand, we did not observe typical, round, pyknotic nuclei
521 in cones in *mak* mutants. Rather, mutant cones progressively shorten after 4 dpf, becoming
522 extremely flattened at 5 dpf, and finally disappearing by 6 dpf. Although we observed
523 TUNEL signals in flattened cone photoreceptors in the central retina at 5 dpf, the
524 degenerative process of cones seems to be different from that of rods in *mak* mutants.

525 Recently, it was reported that photoreceptor degeneration in ciliogenesis-defective
526 zebrafish *Tulp1* mutants is associated with pathological features of ferroptosis (Jia et al.,
527 2022), which is a new form of cell death linked to iron-dependent accumulation of lipid
528 peroxides (Yu et al., 2017), suggesting that ciliogenesis defects may trigger non-apoptotic
529 cell death mechanisms. However, we found that overexpression of anti-apoptotic protein,
530 Bcl2, effectively suppresses degeneration in both rods and cones, suggesting that in *mak*
531 mutants, both depend on Bax-mediated apoptosis. Interestingly, early pyknotic nuclei in
532 presumptive rods and a later progressive flatten-shaped shrinkage of the photoreceptor layer
533 was also observed in zebrafish *oval* and *elipsa* mutants, which show severe defects in
534 axoneme formation by genetic mutation of IFT88 and Traf3ip1, respectively (Bahadori et al.,
535 2003; Doerre and Malicki, 2002; Sukumaran and Perkins, 2009; Wang et al., 2022). It is an
536 interesting question why such a difference in degeneration occurs between rods and cones in
537 zebrafish mutants showing defects in axoneme formation. Recent metabolic transcriptome
538 analysis combined with scRNA-seq revealed that cellular metabolism of rods and cones
539 depends on aerobic glycolysis and oxidative phosphorylation, respectively, but that cones
540 shift toward glycolysis in the early pathological stage of retinitis pigmentosa, suggesting that
541 there is an intrinsic difference of metabolic regulation between rods and cones (Lee et al.,
542 2023). In general, ciliopathy is the common important topic beyond photoreceptor
543 degeneration, but it is still unknown how ciliogenesis defects activate the cell death pathway.

544 Zebrafish *mak* mutants provide a good model to study ciliogenesis-linked cell death
545 mechanisms.

546 **Materials and Methods**

547 **Ethics statement**

548 Zebrafish were maintained at 28.5 °C, on a 14h light/10h dark cycle, following the standard
549 procedure (Westerfield, 2000). Collected embryos were cultured in E3 embryo medium (5
550 mM NaCl, 0.17 mM KCl, 0.33 mM $CaCl_2$, 0.33 mM $MgSO_4$) containing 0.003% 1-phenyl-
551 2-thiouera (PTU) to prevent pigmentation and 0.01% methylene blue to prevent fungal
552 growth. All experiments were performed on zebrafish embryos between the one-cell stage
553 and 6 dpf prior to sexual differentiation. Therefore, sexes of embryos could not be
554 determined. All zebrafish experiments were performed under the OIST Animal Care and Use
555 Program based on the Guide for the Care and Use of Laboratory Animals by the National
556 Research Council of the Nation Academies and has been approved by the Association for
557 Assessment and Accreditation of Laboratory Animal Care (AAALAC). The OIST
558 Institutional Animal Care and Use Committee approved all experimental protocols (Protocol:
559 ACUP-2023-016, ACUP -2023-017, ACUP -2023-018, ACUP -2023-019, ACUP -2023-
560 020).

561

562 **Zebrafish strains and maintenance**

563 Okinawa wild-type (Oki) was used as a wild-type strain to maintain all mutant and transgenic
564 strains. The zebrafish mutant, *pday*^{s351}, was originally isolated by Herwig Baier lab (Muto et
565 al., 2005). Mapping of the *pday*^{s351} mutation was carried out in the genetic background of
566 WIK. Zebrafish transgenic lines, *Tg[gnat2:NLS-tdTomato]*^{oki070} and *Tg[rho: NLS-eGFP]*^{oki071},
567 were used to visualize cone and rod nuclei, respectively. *Tg[hsp:mCherry-Bcl2]*^{oki029}
568 (Nishiwaki and Masai, 2020) was used to express mCherry-tagged zebrafish Bcl2 under
569 control of the zebrafish *heat-shock 70* (*hsp70*) promoter. *Tg[crx:eGFP]*^{oki072}, *Tg[crx:eGFP-*
570 *WT MAK]*^{oki073}, *Tg[crx:eGFP-AR MAK]*^{oki074} and *Tg[crx:eGFP-ADF MAK]*^{oki075}, and
571 *Tg[crx:eGFP-DM MAK]*^{oki076} were used to express eGFP-tagged wild-type and kinase-
572 deficient mutants MAK, respectively. *Tg[gnat2:arl13b-tdTomato]*^{oki077} and *Tg[rho:arl13b-*
573 *eGFP]*^{oki078} were used to visualize cone and rod OSs, respectively.

574

575 **Mapping and cloning of the *pday* mutant gene**

576 *pday*$^{+/-}$ fish maintained in *oki* wild-type background were outcrossed with *WIK* wild-type
577 strain to generate F1 *pday*$^{+/-}$ fish with an *oki* and *WIK* trans-heterozygous wild-type
578 background. These F1 *pday*$^{+/-}$ male and female fish were crossed to produce F2 embryos. F2
579 *pday*$^{-/-}$ embryos were selected by measuring OKR at 5 dpf and stored in methanol at -80 ^{o}C.
580 Genomic DNA was extracted from individual F2 *pday*$^{-/-}$ embryos. First, two DNA pools of
581 20 wild-type and 20 homozygous mutant embryos, respectively, were applied to PCR-
582 mediated amplification of SSLP markers (Knapik et al., 1998; Shimoda et al., 1999) to
583 examine which chromosome hosts the *pday* mutation. Furthermore, 93 F2 *pday*$^{-/-}$ embryos
584 (186 meiosis) were used to restrict the cytogenetic position of the *pday* mutation using SSLP
585 markers mapped on the linked chromosome. After we restricted the *pday* mutation within the
586 genomic region flanked between two SSLP markers, z23011 and z13695, which were
587 annotated at positions 8.517 and 9.123 Mb on chromosome 24 (zebrafish genomic database,
588 GRCz10, Ensemble release 80), we designed a new SSLP marker, namely Mak-N1, which
589 was located around 20 bp upstream of the first exon of the *mak* gene, and confirmed no
590 recombination of Mak-N1 in all 93 F2 *pday*$^{-/-}$ embryos (186 meiosis). Sequence information
591 on forward and reverse primers of z23011, z13695, and Mak-N1 are provided in the appendix.

592 To confirm that *pday* gene encodes MAK, full-length *mak* cDNAs were amplified by
593 PCR using mRNA prepared from wild-type and *pday*^{s351} homozygous embryos at 6 dpf.
594 However, only a partial cDNA fragment that corresponds to the C-terminal coding region
595 covering from the middle of exons 7 to 15 was amplified by PCR from *pday* homozygous
596 mutant mRNA. We sequenced the full-length cDNA of wild type and the C-terminal partial
597 cDNA of *pday* homozygous mutants and found no amino acid change in the MAK coding
598 region from exons 8 to 15 between wild-type and *pday*$^{-/-}$ cDNA. Next, we amplified six DNA
599 fragments from *the pday*$^{-/-}$ genome, each of which covers six N-terminal coding exons (the
600 exon 2 - 7), respectively. Sequencing of these six DNA fragments revealed a non-sense
601 mutation in exon 4 of the *pday*$^{-/-}$ genome. To confirm that the *pday* mutant gene encodes
602 MAK, we combined *pday* mutants with the transgenic line *Tg[crx:eGFP-WT MAK]*^{oki073}, and

603 confirmed that expression of eGFP-tagged MAK in photoreceptor precursors rescues
604 photoreceptor degeneration in *pday* mutants.
605
606 **Generation of DNA expression constructs and their transgenic lines**
607 *Tol2[crx: membrane targeted YFP (MYFP)]* was used as a template to make the expression
608 construct *Tol2[crx: eGFP-MAK]*. *Tol2[crx: MYFP]* was constructed using the To2kit
609 multiple gateway-based construction system (Kwan et al., 2007), whose Tol2 vector
610 backbone contains *cmcl2:CFP* transgenesis marker (Suzuki et al., 2013). *mak* cDNA
611 corresponding to a full-length isoform annotated on the zebrafish genomic database (mak-
612 201, GRCz11, Ensemble release 110), was amplified by PCR using a mRNA pool of 3-dpf,
613 wild-type embryos and was subcloned into pCR TOPO vector (Invitrogen). After the eGFP
614 cDNA fragment was tagged in-frame to the *mak* full-length cDNA at the N-terminus, the
615 MYFP region of *Tol2[crx: MYFP]* was replaced with the DNA fragment encoding eGFP-
616 tagged *mak* cDNA at the *BamHI* and *ClaI* sites, to make the expression construct
617 *pTol2[crx:eGFP-WT MAK]*. The *pTol2[crx:eGFP-WT MAK]* was used as a template in the
618 site-directed mutagenesis for making three kinase-dead MAK constructs, *Tg[crx:eGFP-AR*
619 *MAK]*, *Tg[crx:eGFP-ADF MAK]* and *Tg[crx:eGFP-DM MAK]*.
620 The *EF1α* promoter of Tol2 transposon vector pT2AL200R150G (Urasaki et al.,
621 2006) was replaced with the zebrafish *gnat2* promoter (Iribarne et al., 2019) at the *XhoI* and
622 *BamHI* site to make *Tol2[gnat2:eGFP]*. Zebrafish *arl13b* cDNA was amplified by PCR
623 using an mRNA pool prepared from 4-dpf, wild-type embryos and subcloned into the pCR
624 TOPO vector (Invitrogen). After a tdTomato cDNA fragment was tagged in-frame to the
625 *arl13b* cDNA at the C-terminus, a DNA fragment of tdTomato tagged *arl13b* cDNA was
626 further subcloned into the modified pT2AL200R150G carrying the *gnat2* promoter at the
627 *BamHI* and *ClaI* sites, to make the expression construct *pTol2[gnat2:arl13b-tdTomato]*.
628 Similarly, the *EF1α* promoter of Tol2 transposon vector pT2AL200R150G was replaced
629 with the zebrafish *rhodopsin* promoter (1.1kb upstream of the transcription unit) at the *XhoI*
630 and *BamHI* site. A DNA fragment of C-terminal eGFP-tagged *arl13b* cDNA was prepared

631 and subcloned into the modified pT2AL200R150G carrying *rhodopsin* promoter at the
632 *BamHI* and *ClaI* sites, to make the expression construct *pTol2[rho:arl13b-eGFP]*.
633 The nuclear localization signal (NLS) was fused to cDNA encoding tdTomato or
634 eGFP at the N-terminus. DNA fragments of NLS-tdTomato and NLS-eGFP were subcloned
635 into the modified pT2AL200R150G carrying the zebrafish *gnat2* promoter and the zebrafish
636 *rhodopsin* promoter, respectively, at the *BamHI* and *ClaI* sites, to make the expression
637 constructs *pTol2[gnat2:NLS-tdTomato]* and *pTol2[rho:NLS-eGFP]*.
638 Next, these Tol2 expression construct plasmids and Tol2 transposase mRNA were
639 co-microinjected into one-cell-stage zebrafish fertilized eggs for generation of transgenic
640 lines, *Tg[crx:eGFP-WT MAK], Tg[crx:eGFP-AR MAK], Tg[crx:eGFP-ADF MAK],*
641 *Tg[crx:eGFP-DM MAK], Tg[gnat2:arl13b-tdTomato], Tg[rho:arl13b-eGFP],*
642 *Tg[gnat2:NLS-tdTomato]* and *Tg[rho:NLS-eGFP]*. Injected F0 fish expressing fluorescent
643 protein (eGFP or tdTomato) in the ONL were bred until adulthood and used to identify
644 founder fish, which produce fluorescent protein-expressing F1 progeny. These transgenic F1
645 embryos were raised and used to produce F2 generation for establishment of the transgenic
646 strain.
647
648 **Histology**
649 For plastic section, zebrafish embryos were anesthetized in 0.02% 3-aminobenzoic acid ethyl
650 ester (tricaine) and fixed in PBS (150mM NaCl, 10mM $PO4^{3-}$, pH 7.4) (Invitrogen) with 4%
651 paraformaldehyde (PFA) at 4 ^{o}C overnight. Samples were dehydrated with an ethanol
652 gradient before being embedded in JB4 resin (Polysciences). Samples were sectioned at 5
653 μm with a microtome Rotatif, NM335E (MICROM International GmbH) and stained with
654 0.02% toluidine blue for further analysis.
655 For TUNEL, samples were covered with the staining mixture at 37 ^{o}C for 1 h
656 following instructions of the In Situ Cell Death Detection Kit (Roche, 11684795910). After
657 the TUNEL reaction, nuclei were stained with 60 mM PO_4 buffer (PB) (42.6 mM NaH_2PO_4,
658 17.4 mM Na_2HPO_4, pH 7.3) containing Hoechst 33342 (Fujifilm, 346-07951) at 1:1000,

659 followed by washing with PB with 0.1% TritonX-100 (0.1% PBTx) for 3 x 5 min. Samples
660 were mounted with Fluoromount (Diagnostic BioSystems, K024) for further analysis.
661 For immunohistochemistry, 3-6-dpf embryos were fixed with 4 % PFA at 4 °C
662 overnight, and transferred to 30% sucrose in PB overnight before being embedded and frozen
663 in OCT compound. Cryosections was prepared at 7 μm with a cryostat (Cryostar NX70,
664 Thermo Scientific.), except at 20 μm for imaging cilia components. Cryosections were air-
665 dried for at least 2 h, then rehydrated in 0.1% PBTx for 3 x 5 min. Rehydrated sections were
666 immersed in blocking solution (10% goat serum in 0.1% PBTx) for 1 h at room temperature,
667 then applied to the primary antibody in the blocking solution at an appropriate dilution (see
668 appendix), and washed with 0.1% PBTx 3 x 10 min. Next, primary antibody-labeled sections
669 were applied to the fluorophore-conjugated secondary antibody at 1:500 and Hoechst 33342
670 (DOJINDO Laboratories, CAS23491-52-3) or 50 nM Sytox-Green (Molecular Probes) in
671 blocking solution for 1 h at room temperature, and then washed with 0.1% PBTx 3 x 10 min.
672 Sections were finally mounted with Fluoromount. Confocal images were scanned with
673 confocal laser-scanning microscopes, LSM780 (Carl Zeiss) or Fluoview FV3000 (Olympus,
674 Evident).
675 For EM analysis, 3-dpf embryos were fixed in PB with fixative (2.5% glutaraldehyde,
676 1% paraformaldehyde, 3% sucrose, and 30 mM HEPES) on ice for 2 h, followed by washing
677 with PB with 3% sucrose and 30 mM HEPES 3 x 5 min. Embryos were postfixed in 60 mM
678 PB with 1% OsO_4 for 1 h on ice, followed by washing with Milli-Q water three times.
679 Samples were dehydrated with a gradient series of ethanol and replaced by acetone. After
680 treatment with a gradient series of propylene oxide (PO), epoxy resin EPON812 (Nisshin-
681 EM, 3402) was applied to the samples before they were embedded in resin and solidified for
682 2 days at 60 °C. Ultra-thin sections at 50 nm were prepared with a Leica UC7 ultra-microtome
683 and processed with Reynolds' stain (Reynolds, 1963). Images were observed and captured
684 using a JOEL JEM-1230R transmission EM.
685
686 **Bcl2 overexpression in *pday* mutant retinas**

687 Transgenic line *Tg[hsp:mCherry-Bcl2]* (Nishiwaki and Masai, 2020) was combined with
688 *pday* mutants. Heat shock treatment was carried out by incubation of embryos at 39 °C for 1
689 h every 12 h after 1 dpf until 6 dpf.
690
691 ***In situ* hybridization**
692 Whole-mount *in situ* hybridization was carried out using a published protocol (Thisse and
693 Thisse, 2008). A DNA fragment containing *mak* full-length cDNA combined with T7 RNA
694 polymerase promoter, which is located at the 3' end of the *mak* full-length cDNA, was
695 amplified by PCR. Digoxigenin (DIG)-labeled anti-sense *mak* RNA probe was generated by
696 *in vitro* transcription from this T7 promoter: *mak* cDNA fragment as the template using a
697 DIG RNA labeling kit (Roche, 11175025910). Zebrafish embryos from the 1-cell stage to 72
698 hpf were fixed with 4% PFA at 4 °C overnight, and were stored in 100 % methanol at -70 °C.
699 Samples were rehydrated from methanol to PBS, and then treated with protenase K (10
700 μg/mL) to increase permeability. After refixing with 4% PFA for 20 min, samples were
701 soaked with prehybridization buffer at 65 °C for 2 h, then incubated with hybridization buffer
702 containing *mak* antisense RNA probe at 65 °C overnight. Samples were washed with 2xSSC
703 with 0.1 % Tween20 for 5 min, room temperature, and then 0.2xSSC with 0.1 % Tween20 3
704 x 30 min at 65 °C. Washed samples were transferred to maleic acid buffer with 0.1%
705 Tween20 (MABT), and then to MABT with 2% blocking reagent (Roche, 11096176001) at
706 4°C overnight. Samples were incubated with anti-DIG-AP antibody (Roche, 11093274910)
707 at 1:6,000 in MABT for 1 h at room temperature, washed with MABT 3 x 15 min, and then
708 transferred to Tris-HCl buffer (pH 9.5) for 15 min. For alkaline phosphatase (AP) reaction,
709 samples were transferred to BM-Purple (Roche, 11442074001) until a blue signal developed,
710 and fixed with 4% PFA overnight at 4 °C. These samples were mounted in 70% glycerol-
711 PBS and stored at 4 °C for long-term preservation. Images of the embryos were observed
712 with a SteREO Discovery V12 dissection microscope (Carl Zeiss).
713
714 **Live imaging**

715 For live imaging using confocal LSM, embryos were anesthetized in 0.02% tricaine and
716 mounted on glass slides in appropriate positions and glued with 3% methylcellulose. An
717 upright confocal LSM, FV3000 (Olympus, Evident) was used for scanning fluorescent
718 signals in the photoreceptor OS of *Tg[crx:GFP-MAK]*.
719
720 ***In vitro* kinase assay**
721 The wild-type zebrafish *mak* cDNA fragment was introduced into pGEX6p3 (GE Health
722 Care Life Science). Kinase-dead *mak* cDNA fragments were generated from pGEX6p3-
723 zMAK(wt) with primers for site-directed mutagenesis. Plasmids were transformed into *E.*
724 *coli* strain BL21-competent cells (TaKaRa Bio, TKR9126). Colonies were inoculated into
725 LB broth for starter cultures incubated at 37 ^{o}C overnight, followed by amplification cultures
726 containing 1% of the starters. Amplification cultures were cooled on ice once the O.D.
727 reached 0.6 and IPTG was added (TaKaRa Bio, TKR9030) to a final concentration of 1 mM,
728 and incubated at 20 ^{o}C overnight. Cultures were pelleted, washed with cold PBS, and
729 sonicated in 1% PBS TritonX-100 (PBSTx) with 1x protease inhibitor (Roche,
730 04693132001). Debris was then pelleted, and supernatant fractions were subjected to
731 Glutathione Sepharose 4B (Cyvita, 17-0756-01) for 1.5 h at 4 ^{o}C. After being washed with
732 cold PBS 3x, Sepharose beads were incubated with PreScission protease (Cyvita, 27084301)
733 in the solution at 4 ^{o}C to release MAK from the GST tag. Digested products were pelleted,
734 and supernatant fractions were used for *in vitro* kinase assays.
735 Each reaction for *in vitro* kinase assays is composed of 50 mM Tris-HCl (pH 7.0), 10
736 mM $MgCl_2$, 5 mM ATP (Thermo Scientific, R0441), 1 mM DTT (Thermo Scientific, 20290),
737 5 μg dephosphorylated myelin basic protein (Merck, 13-110), and purified MAK protein.
738 Reactions were incubated 1 h at 30 ^{o}C. Samples were mixed with SDS sample dye and
739 incubated for 20 min at 75 ^{o}C to stop the reactions. Samples were separated by SDS-PAGE
740 and transferred onto a PVDF membrane for later analyses. The membrane was blocked with
741 5% skim milk for 1 h at room temperature followed by probing with primary antibodies and
742 HRP-conjugated secondary antibodies. ECL substrate (Thermo Scientific, 34577) was
743 applied to visualize signals using a iBright FL1500 imager (Invitrogen).

744

745 **Data quantification and statistical analysis**

746 To qualify the thickness of photoreceptor layers, photoreceptor layers in the images were
747 straightened with the straighten tool of ImageJ (Fig. S5A). A line dividing the photoreceptor
748 layer into 10 parts was generated with Adobe Illustrator. The photoreceptor layer thickness
749 at each decile was measured with ImageJ by following the conversion ratio of pixels to the
750 actual length of the scale bar. To qualify photoreceptor numbers, photoreceptor layers in the
751 images were straightened with ImageJ, and a reference line marking every 1/10 points was
752 drawn with Adobe Illustrator. Cell numbers were manually counted. TUNEL signals in
753 retinas were manually counted. The zpr1-positive area in the total retinal was calculated as
754 previously described (Fig. S5B) (Nishiwaki et al., 2013). All statistical analyses were
755 performed with GraphPad Prism 9.2.1. Significance levels, numbers of samples, and the
756 details of analyses are indicated in each figure and figure legend.

757 **Acknowledgments**
758 We are grateful to Herwig Baier and Akira Muto for providing the *pday* mutant line. We also
759 thank Tadashi Yamamoto for providing the vector, pGEX6p3. We thank previous lab
760 members, Brandy Lee Denis and Maria Iribarne for supporting the experiment to clone *pday*
761 mutant gene, Shohei Suzuki for cloning of the zebrafish *rhodopsin* promoter, Sachihiro
762 Suzuki for cloning of the zebrafish *gnat2* promoter, Yutaka Kojima, Ayano Harata and
763 Hiroshi Izumi for supporting histological analyses of *pday* mutant phenotypes. We are
764 grateful to the Imaging Section and the sequencing section of the Research Support Division
765 of OIST. We thank Steven D. Aird for critical reading and editing of the manuscript.
766
767 **Data availability**
768 N/A
769
770 **Author contributions statement**
771 Conceptualization: H-JC, IM; Methodology: H-JC, YN, IM; Software: H-JC, IM; Validation:
772 H-JC, YN, W-CC, IM; Formal analysis: H-JC, YN, IM; Investigation: H-JC, YN, W-CC,
773 IM; Resources: H-JC, YN, W-CC, IM; Data curation: H-JC, YN, W-CC, IM; Writing -
774 original draft: H-JC, IM; Writing - review & editing: H-JC, IM; Visualization: H-JC, YN,
775 W-CC, IM; Supervision: IM; Project administration: H-JC, YN, IM; Funding acquisition:
776 IM.
777
778 **Funding**
779 This work was funded by a grant from the Okinawa Institute of Science and Technology
780 Graduate University to IM.
781
782 **Declaration of interests**
783 The authors declare no competing interests.

784 **Figure Legends**

785 **Fig. 1: Zebrafish *pday* mutants carry a non-sense mutation in the *mak* gene and show**
786 **photoreceptor degeneration.**

787 (A) *pday* mutants at 6 dpf and 2 mpf. At 6 dpf, *pday* mutants show no morphological
788 differences from wild-type siblings. At 2 mpf, *pday* mutants show smaller body size with
789 less well-developed fins, scoliosis, and cardiac edema (open arrowhead). Scale bars: 200
790 μm.

791 (B) The zebrafish *mak* gene consists of 15 exons and encodes 633 amino acids with a
792 serine/threonine kinase domain. A non-sense mutation occurs in exon 4 of *mak* gene in
793 *pday* mutants, leading to a premature termination codon at 70R, resulting in a truncated
794 protein lacking most of serine/threonine kinase domain.

795 (C) Wild-type and *pday* mutant retinas at 3, 4, 5 and 6 dpf. The ONL in *pday* mutants shows
796 dense nuclear granules (yellow arrowheads), bubble-like structures (red arrowheads) and
797 reduced outer segments (yellow lines). In *pday* mutants, the dorso-central ONL is
798 progressively decreased in thickness after 4 dpf, becomes extremely flat at 5 dpf and
799 disappears at 6 dpf (red dotted lines). On the other hand, other retinal layers, INL, IPL,
800 RGCL are maintained in *pday* mutants.

801 (C') Higher-magnification images of the central ONL. The OS is drastically reduced in *pday*
802 mutants (red lines). Dense nuclear granules (yellow arrowheads) and bubble-like
803 structures (red arrowheads) are observed in *pday* mutants. The ONL thickness is
804 progressively reduced in *pday* mutants (yellow lines). HC, horizontal cells; PR,
805 photoreceptors.

806 (D) Wild-type and *pday* mutant retinas at 6 dpf carrying the transgenic line *Tg[crx:eGFP]*.
807 Nuclei were counterstained with Hoechst 33342 (blue). crx:eGFP (green) expression is
808 more severely decreased in the dorsal region (red dotted line) than in the ventral region
809 of *pday* mutant retinas.

810 (E) Histogram of thickness of eGFP-positive photoreceptors along the DV axis of the retina.
811 The thickness of photoreceptors is more severely decreased in the dorsal region than in
812 the ventral region of *pday* mutant retinas. Color bars and lines indicate mean ± SD.

813 Statistical difference is evaluated with 2-way ANOVA and Sidak's multiple comparison
814 tests, n=3 for each point. ** $p<0.01$, *** $p<0.001$, **** $p<0.0001$.
815 Scale bars: 200 μm (A), 50 μm (C), 10 μm (C'), 40 μm (D).
816
817 **Fig. 2: Rods undergo apoptotic-like degeneration in *pay* mutants, whereas cones**
818 **progressively shrink.**
819 (A-B) Wild-type and *pday* mutant retinas carrying the transgenic lines *Tg[rho:NLS-eGFP]*
820 and *Tg[gnat2:NLS-tdTomato]*, which visualize rods (green) and cones (red),
821 respectively. Nuclei were counterstained with Hoechst 33342 (blue). (A) Only green and
822 blue channel. (B) Only red and blue channel. Squares indicate the dorsal and ventral
823 ONL, shown in (C–F).
824 (C) The dorsal ONL of wild-type and *pday* mutant retinas with *Tg[rho:NLS-eGFP]*, which
825 visualizes rods (green). In *pday* mutants, rods have condensed, round nuclei (white
826 arrowheads) at 3 dpf, which resembles apoptosis. In *pday* mutants, rods are drastically
827 reduced in number at 4 dpf and disappeared at 5 and 6 dpf (asterisks), except in the
828 peripheral region near the dorsal CMZ.
829 (D) The ventral ONL of wild-type and *pday* mutant retinas with *Tg[rho:NLS-eGFP]*, which
830 visualizes rods (green). In *pday* mutants, rods have condensed, round nuclei (white
831 arrowheads) at 3 and 4 dpf. However, in *pday* mutants, rods disappeared at 5 and 6 dpf
832 (asterisks), except in the peripheral region near the ventral CMZ.
833 (E) The dorsal ONL of wild-type and *pday* mutant retinas with *Tg[gnat2: NLS-tdTomato]*,
834 which visualizes cones (red). In wild type, cones form monolayer at 3 dpf and two
835 subnuclear layers after 4 dpf. In *pday* mutants, cones form monolayer at 3 dpf; however,
836 tdTomato-negative nuclei are observed, whose position is identical to that of condensed
837 rod nuclei (white arrowheads). From 4 to 5 dpf, cones shrink progressively and become
838 flattened (yellow line). At 6 dpf, cones are extremely flattened and disappear, leaving
839 gaps (yellow arrowheads), except in the peripheral region near the dorsal CMZ.
840 (F) The ventral ONL of wild-type and *pday* mutant retinas with *Tg[gnat2: NLS-tdTomato]*,
841 which visualizes cones (red). In wild type, cones differentiate at 3 dpf but progressively

842 disappear toward the peripheral area of the ventral ONL, where rods densely differentiate.
843 In *pday* mutants, the ONL thickness is progressively decreased after 4 dpf. Interestingly,
844 after 5 dpf, the cone differentiating area is expanded toward the periphery of the ventral
845 ONL (asterisks), where rods disappear.
846 (G) Schematic drawing of cone and rod degeneration in *pday* mutants. Rods undergo acute
847 degeneration with apoptotic-like pyknotic nuclei during 3 - 4 dpf, whereas cones undergo
848 progressive shrinkage of cell volume during 4 - 6 dpf and disappear by 6 dpf.
849
850 **Fig. 3: Rods and cones undergo apoptosis in *pday* mutants.**
851 (A) TUNEL of wild-type and *pday* mutant retinas at 3, 4, and 5 dpf. TUNEL signals are
852 indicated in red. Nuclei are counterstained with Sytox-Green (green).
853 (A') Higher-magnification images of dorsal, central, and ventral ONL of *pday* mutant retinas,
854 which are indicated by white squares in (A). White arrowheads indicate TUNEL signals
855 (red). TUNEL signals are prominent in the central and ventral ONL at 3 dpf, and in the
856 dorsal and central ONL at 4 dpf. TUNEL signals are detected in a very thin central ONL
857 of *pday* mutants at 5 dpf, where only cones are maintained.
858 (B) Double labeling of 5-dpf wild-type and *pday* mutant retinas with zpr1 (red) and anti-
859 rhodopsin (green) antibodies.
860 (B') Higher-magnification images of dorsal, central, and ventral ONL of *pday* mutant retinas,
861 which are indicated by white squares in (B). Rhodopsin signals are observed only in the
862 peripheral region of the dorsal and ventral ONL (yellow arrowheads). zpr1 signals are
863 also detected in the peripheral ONL; however, zpr1-positive flattened cells are located
864 in the central ONL (white arrow).
865 (C) TUNEL (green) of 5-dpf wild-type and *pday* mutant retinas combined with zpr1 antibody
866 labeling (red).
867 (C') Higher-magnification images of dorsal, central, and ventral ONL of *pday* mutant retinas,
868 indicated by white squares in (C). TUNEL signals are detected in dorsal, central, and
869 ventral ONL, many of which are associated with zpr1 signals (white arrows). A few
870 TUNEL signals are not associated with zpr1 (white arrowheads).

871 (D) TUNEL (red) of 5-dpf wild-type and *pday* mutant retinas combined with anti-rhodopsin
872 antibody labeling (green).
873 (D') Higher-magnification images of dorsal, central, and ventral ONL of *pday* mutant retinas,
874 indicated by white squares in (D). Rhodopsin signals are detected in the peripheral region
875 of dorsal and ventral ONL (yellow arrowheads). TUNEL signals are detected in the
876 dorsal, central, and ventral ONL. TUNEL signals associated with rhodopsin signals are
877 observed only the peripheral region of the dorsal and ventral ONL (white arrowheads).
878 TUNEL signals are not associated with rhodopsin signals in central ONL and non-
879 peripheral region of dorsal and ventral ONL (white arrows).
880 (E, F) Wild-type and *pday* mutant retinas with and without the transgenic line *Tg[hsp:*
881 *mCherry-Bcl2]*, labelled with zpr1 (E) and zpr3 (F) antibodies. Nuclei were
882 counterstained with Hoechst 33342 (blue). zpr1 and zpr3 signals are markedly reduced
883 in non-transgenic *pday* mutant retinas. However, after heat-shock treatment, zpr1 and
884 zpr3 signals in the ONL are recovered in *pday* mutant retinas with *Tg[hsp: mCherry-*
885 *Bcl2]* (white arrowheads).
886 (F') Higher-magnification images of the dorsal ONL indicated by white squares, shown in
887 (F). zpr3 signals are localized in the OS of wild type, but ectopically distributed outside
888 the OS in *pday* mutants.
889 Scale bars: 50 μm (A-D), 40 μm (E, F)
890
891 **Fig. 4: Overexpression of MAK restores survival and visual function of *pday* mutant**
892 **photoreceptors.**
893 (A) Labeling of wild-type and *pday* mutant retinas with zpr1 (red) and anti-eGFP (green)
894 antibodies carrying transgenic line *Tg[crx:eGFP]* or *Tg[crx:eGFP-MAK]*. Nuclei were
895 counterstained with Hoechst 33342 (blue). (A') indicates only red channel. zpr1 signals
896 are markedly decreased in the dorso-central region of *pday* mutant retinas carrying
897 transgene *Tg[crx:eGFP]* (white dotted lines), but maintained in *pday* mutant retinas
898 carrying transgene *Tg[crx:eGFP-MAK]*.

899 (B) The fraction of zpr1-positive area in the total retinal area in wild-type and *pday* mutants
900 with *Tg[crx:eGFP]* or *Tg[crx:eGFP-MAK]*. The fraction is markedly reduced in *pday*
901 mutants with *Tg[crx:eGFP]* (red bar), compared with wild-type siblings with
902 *Tg[crx:eGFP]* (blue bar). However, the fraction is recovered in *pday* mutants with
903 *Tg[crx:eGFP-MAK]* (purple bar), equivalent to wild-type with *Tg[crx:eGFP-MAK]*
904 (green bar). Bars and lines indicate mean ± SD. Statistical significance was evaluated
905 with ordinary one-way ANOVA and Turkey's multiple comparison tests; *p<0.0332,
906 ****p<0.0002, ns: not significant.
907 (C) The fraction of OKR^+ and OKR^- embryos relative to total progeny produced by crosses
908 of $pday^{+/-}$ parent fish (blue), $pday^{+/-}$ parent fish carrying *Tg[crx:eGFP]* (red), and $pday^{+/-}$
909 parent fish carrying *Tg[crx:eGFP-MAK]* (green). 100% of embryos produced by crosses
910 of $pday^{+/-}$ parent fish carrying *Tg[crx:eGFP-MAK]* (green) are positive for OKR. Bars
911 and lines indicate mean ± SD. Statistical significance was evaluated with 2-way ANOVA
912 and Turkey's multiple comparison tests. *** p<0.0002, ns: not significant.
913 Scale bars: 20 μm (A, A')
914
915 **Fig. 5: MAK is localized in axonemes of photoreceptor cilia.**
916 (A) Whole-mount *in situ* hybridization of zebrafish wild-type embryos with *mak* RNA probe.
917 *mak* mRNA is ubiquitously expressed in one-cell- to four-cell stage, but disappears at the
918 50% epiboly stage. *mak* mRNA is expressed in a spot-like region at the most posterior
919 side of tail-bud-stage embryos, which corresponds to Kupffer's vesicle (red open
920 arrowhead). At 24 pf, *mak* mRNA is weakly expressed in the whole body, and strongly
921 expressed in retina and epiphysis (pineal eye) (red open arrowhead). At 48 hpf, *mak*
922 mRNA is expressed in the brain, including retina and pectoral fin. At 72 hpf, *mak* mRNA
923 is expressed in the optic tectum and retina. Retinal expression is restricted to the
924 photoreceptor layer (yellow arrowheads). kv, Kuffper's vesicle; re, retina; epi, epiphysis;
925 br, brain; fin, pectoral fin; Tc, optic tectum; PR, photoreceptor layer.
926 (B) Confocal live image of wild-type *Tg[crx: eGFP-MAK]* transgenic retina at 5 dpf. eGFP-
927 MAK is localized in the OS of photoreceptors (yellow arrowheads).

928 (C) Labeling of 5-dpf, wild-type *Tg[crx: eGFPMAK]* transgenic retina with anti-acetylated
929 α-tubulin (red) and anti-eGFP (green) antibodies. Nuclei were counterstained with
930 Hoechst 33342 (blue). The right panel indicates higher magnification of the square shown
931 in the left panel. eGFP-MAK is localized in the axoneme (white open arrowheads, right
932 panel).
933 Scale bars: 200 μm (A), 5 μm (B, C left), and 1 μm (C, right).
934
935 **Fig. 6: The axoneme is absent, but the basal body and transition zone are formed in**
936 ***pday* mutant photoreceptors.**
937 (A) 3-dpf wild-type and *pday* mutant retinas with anti-acetylated α-tubulin (red) and anti-
938 Eys (green) antibodies. Nuclei were counterstained with Hoechst 33342 (blue). Bottom
939 panels are higher magnification of the ONL shown in top panels. In *pday* mutants,
940 acetylated α-tubulin signal is absent.
941 (B) 3-dpf wild-type and *pday* mutant retinas with anti-γ-tubulin (red) and anti-Eys (green)
942 antibodies. Nuclei were counterstained with Hoechst 33342 (blue). Bottom panels are
943 higher magnification of the ONL shown in top panels. In *pday* mutants, both γ-tubulin
944 and Eys signals are detected.
945 (C) 3-dpf wild-type and *pday* mutant retinas combined with the transgenic lines, *Tg[gnat2:*
946 *arl13b-tdTomato]* and *Tg[rho: ail13b-eGFP]*, which visualize cone OS (red) and rod
947 OS (green), respectively. Nuclei were counterstained with Hoechst 33342 (blue). Bottom
948 panels are higher magnification of the ONL. In *pday* mutants, arl13b signal is absent in
949 both cones and rods.
950 (D-E) EM analysis of wild-type (D) and *pday* mutant (E) photoreceptors at 3 dpf. Bottom
951 panels indicate higher-magnification (3000x) images of apical region of photoreceptors
952 in wild-type siblings (D') and *pday* mutants (E'). Bottom right panels are enlarged
953 images of the square region shown in the bottom left panels. In wild-type photoreceptors,
954 the OS starts to form (red asterisks). Basal body (red arrowheads) and ciliary axoneme
955 (yellow arrowheads) are observed at the basal area of the OS. In *pday* mutants, the OS

956 is absent; however, basal body (red arrowheads) and short ciliary extension from the
957 basal body (orange arrowheads) are observed.
958 (F-G) Labeling of 3-dpf, wild-type and *pday* mutant retinas with zpr3 antibody (F) and 1D4
959 antibody (G), which label rhodopsin/green opsin and red opsin, respectively. Nuclei
960 were counterstained with Hoechst 33342 (blue). Bottom panels are higher magnification
961 of the ONL. Both zpr3 and 1D4 signals are localized in the OS of wild-type
962 photoreceptors, but mislocalized in the apico-most region corresponding to the IS as well
963 as plasma membrane including synaptic area (arrowheads) in *pday* mutant
964 photoreceptors.
965 Scale bars: 5 μm (top panels of A, B, C; bottom panel of F, G), 1 μm (bottom panels of A,
966 B, C; D), and 20 μm (top panels of F, G)
967
968 **Fig. 7: MAK kinase activity is required for MAK protein localization in the ciliary**
969 **axoneme, axoneme formation, and photoreceptor maintenance.**
970 (A) A scheme of generation of three types of MAK kinase-dead mutants: AR MAK, ADF
971 MAK and DM MAK. Zebrafish MAK has a catalytic domain in the N-terminal region,
972 which contains an ATP binding motif, KR, and autophosphorylation site, TDY. AR MAK
973 and ADF MAK were generated by conversion of KR and TDY into AR and ADF,
974 respectively. DM MAK has both AR and ADF mutations.
975 (B) *In vitro* kinase assay of MAK using a substrate, MBP. Only wild-type MAK
976 phosphorylates MBP.
977 (C) Labeling of 6-dpf, wild-type ONL carrying the transgenic line, *Tg[crx:eGFP],*
978 *Tg[crx:eGFP-WT MAK], Tg[crx:eGFP-AR MAK], Tg[crx:eGFP-ADF MAK]*, or
979 *Tg[crx:eGFP-DM MAK]*, with anti-GFP antibody (green). Nuclei were counterstained
980 with Hoechst 33342 (blue). eGFP is ubiquitously localized in cytoplasmic area of
981 *Tg[crx:eGFP]* photoreceptors, but in the ciliary axoneme of *Tg[crx:eGFP-WT MAK]*
982 photoreceptors. However, eGFP is localized in a spot region of *Tg[crx:eGFP-AR MAK]*
983 photoreceptors, which corresponds to the basal area of the OS. eGFP expression is

984 observed in the ciliary axoneme, but reduced in *Tg[crx:eGFP-ADF MAK]* photoreceptors.
985 eGFP expression is markedly reduced in *Tg[crx:eGFP-DM MAK]* photoreceptors.
986 (D) Labeling of 6-dpf, wild-type and *pday* mutant retinas carrying the transgenic line,
987 *Tg[crx:eGFP], Tg[crx:eGFP-WT MAK], Tg[crx:eGFP-AR MAK], Tg[crx:eGFP-ADF*
988 *MAK],* or *Tg[crx:eGFP-DM MAK]*, with zpr1 (red) and anti-GFP (green) antibodies.
989 Nuclei were counterstained with Hoechst 33342 (blue). zpr1-positive photoreceptors are
990 degenerated in dorso-central retinas of *pday* mutants carrying *Tg[crx:eGFP]* (white
991 dotted line). However, photoreceptor degeneration is rescued only in *pday* mutants
992 carrying *Tg[crx:eGFP-WT MAK]*, but not in *pday* mutants carrying kinase-dead mutant
993 transgenes (white dotted line).
994 (E) Labeling of 3 dpf wild-type and *pday* mutant ONL carrying the transgenic line,
995 *Tg[crx:eGFP], Tg[crx:eGFP-WT MAK], Tg[crx:eGFP-AR MAK], Tg[crx:eGFP-ADF*
996 *MAK],* or *Tg[crx:eGFP-DM MAK]*, with anti-acetylated α-tubulin antibody (red). Nuclei
997 were counterstained with Hoechst 33342 (blue). Axoneme formation defects are rescued
998 only in *pday* mutants carrying *Tg[crx:eGFP-WT MAK]* (arrowheads), but not in *pday*
999 mutants carrying kinase-dead mutant transgenes (asterisks).
1000 Scale bars: 5 μm (C, E) and 40 μm (D).
1001
1002 **Fig. 8: MAK is essential for ciliary axoneme formation in zebrafish photoreceptor**
1003 **ciliogenesis.**
1004 (A) A possible role of MAK in ciliogenesis in zebrafish photoreceptors. During ciliogenesis,
1005 MAK promotes axoneme extension following formation of the transition zone through
1006 phosphorylation of its substrate proteins.
1007 (B) Phenotypes of zebrafish *mak* mutant photoreceptors. In the absence of MAK, the
1008 axoneme does not form, resulting in failure to form the OS and to transport
1009 phototransduction molecules into the OS.
1010

1011 **Supplementary Figure Legends**

1012 **Fig. S1: Visualization of rods and cones in *pday* mutants.**

1013 (A) Confocal images of wild-type (the left column) and *pday* mutant retinas (middle column)
1014 carrying the transgenes *Tg[rho:NLS-eGFP]* and *Tg[gnat2:NLS-tdTomato]*, which
1015 visualize rods (green) and cones (red), respectively. Nuclei were counterstained with
1016 Hoechst 33342 (blue). In *pday* mutant retinas, eGFP signals are weak. The right column
1017 indicates confocal scanning images of *pday* mutant retinas carrying the transgenes
1018 *Tg[rho:NLS-eGFP]* and *Tg[gnat2:NLS-tdTomato]*, with higher laser intensity, to
1019 enhance eGFP signals. We compare wild-type and *pday* mutant retinas in conventional
1020 scanning conditions and with higher laser intensity, respectively, in Figure 2. Scale bars:
1021 40 μm.

1022 (B) Histogram of rod number of wild-type siblings (black) and *pday* mutants (red) retinas at
1023 3, 4, 5 and 6 dpf. Rod number was counted in 1/10th divided area of the ONL along the
1024 DV axis and analyzed with 2-way ANOVA and Sidak's multiple comparison tests, n=3
1025 for wild-type, n=4 for *pday* mutants at 3 dpf; n=4 for wild-type, n=5 for *pday* mutants at
1026 4 dpf; n=3 for wild-type, n=3 for *pday* mutants at 5 dpf; n=4 for wild-type, n=4 for *pday*
1027 mutants at 6 dpf. Bars and lines indicate mean ± SD. * $p<0.02$, ** $p<0.003$, ****
1028 $p<0.0001$, ns: not significant.

1029

1030 **Fig. S2: Statistical analysis of TUNEL and Bcl2-mediated rescue of photoreceptor**
1031 **phenotypes in *pday* mutants.**

1032 (A) The number of TUNEL signals in wild-type and *pday* mutant ONL at 3, 4, and 5 dpf.
1033 TUNEL signals in the ONL are higher in *pday* mutants than in wild type at 3 dpf, although
1034 the difference is not significant. TUNEL signals in the ONL are the highest in *pday*
1035 mutants at 4 dpf and are still significantly higher in *pday* mutants at 5 dpf, compared with
1036 wild-type siblings. Bars and lines indicate mean ± SD. Statistical significance was
1037 evaluated with 2-way ANOVA and Sidak's multiple comparison tests; * $p<0.03$, ****
1038 $p<0.0001$, ns: not significant.

1039 (B) The number of TUNEL signals in wild-type and *pday* mutant INL at 3, 4, and 5 dpf.
1040 TUNEL signals in the INL are higher in *pday* mutants than in wild type at 4 dpf, although
1041 the difference is not significant. Bars and lines indicate mean ± SD. Statistical
1042 significance was evaluated with 2-way ANOVA and Sidak's multiple comparison tests;
1043 ns: not significant.
1044 (C) The number of TUNEL signals in wild-type and *pday* mutant RGCL at 3, 4, and 5 dpf.
1045 There is no significant difference between wild-type and *pday* mutants at any stage. Bars
1046 and lines indicate mean ± SD. Statistical significance was evaluated with 2-way ANOVA
1047 and Sidak's multiple comparison tests; ns: not significant.
1048 (D) The fraction of zpr1-positive area in the total retinal in wild-type and *pday* mutants
1049 without and with mCherry-Bcl2 overexpression. The fraction of the zpr1-positive area is
1050 markedly reduced in *pday* mutants (red bar), compared with wild-type siblings (blue bar).
1051 However, the fraction of the zpr1-positive area is recovered in *pday* mutants with
1052 mCherry-Bcl2 overexpression (purple bar), equivalent to wild-type without (blue bar)
1053 and with mCherry-Bcl2 overexpression (green bar). Bars and lines indicate mean ± SD.
1054 Statistical significance was evaluated with 2-way ANOVA and Turkey's multiple
1055 comparison tests; *$p<0.0332$, **$p<0.0021$, ns: not significant.
1056 (E) The fraction of the zpr3-positive area in the total retinal area in wild-type and *pday*
1057 mutants without and with mCherry-Bcl2 overexpression. The fraction of the zpr3-
1058 positive area is markedly reduced in *pday* mutants (red bar), compared with wild-type
1059 siblings (blue bar). However, the fraction of the zpr3-positive area is recovered and
1060 increased in *pday* mutants with mCherry-Bcl2 overexpression (purple bar), compared
1061 with wild-type without (blue bar) and with mCherry-Bcl2 overexpression (green bar),
1062 probably due to ectopic distribution of zpr3 signals outside the OS. Bars and lines indicate
1063 mean ± SD. Statistical significance was evaluated with 2-way ANOVA and Turkey's
1064 multiple comparison tests; **$p<0.0021$, ***$p< 0.0002$, ****$p<0.0001$, ns: not significant.
1065 (F) Histogram of zpr1-positive cone thickness in *pday* mutant retinas with (blue) and without
1066 (red) overexpression of mCherry-Bcl2. The ONL is divided into 10th area along the DV
1067 axis. zpr1-positive cone thickness was measured at the interface between each

1068 neighboring region and evaluated with 2-way ANOVA and Sidak's multiple comparison
1069 tests, n=3 for *pday* mutants, n=4 for *pday* mutants with *Tg[hsp:mCherry-Bcl2]*. **
1070 p<0.003, *** p<0.001, **** p<0.0001. Bars and lines indicate mean ± SD.
1071 (G) Nuclear labeling of wild-type and *pday* mutant ONL overexpressing mCherry-Bcl2 with
1072 Hoechst 33342. Nuclear shape in the ONL is slightly irregular in *pday* mutants
1073 overexpressing Bcl2.
1074 (H) The percentage of OKR+ and OKR- embryos produced by crosses of *pday* heterozygous
1075 male and female fish without (red) and with the transgene *Tg[hsp:mCherry-Bcl2]* (blue).
1076 There is no significant difference between the absence and the presence of
1077 *Tg[hsp:mCherry-Bcl2]*. Statistical difference as evaluated with 2-way ANOVA and
1078 Sidak's multiple comparison tests. Bars and lines indicate mean ± SD, ns: not significant.
1079 Scale bars: 5 μm (G).
1080
1081 **Fig. S3: MAK is localized in ciliary axoneme.**
1082 Projection view of 3D confocal image of wild-type transgenic *Tg[crx: eGFP-MAK]* ONL
1083 with anti-GFP and anti-acetylated tubulin antibodies. Nuclei were counterstained with
1084 Hoechst 33342. Left panel indicates a radially sectioned projection view of the retina. The
1085 eGFP-MAK signals overlap with anti-acetylated α-tubulin signals. Right panel indicates
1086 tangentially sectioned projection view, which was digitally produced by rotating the radially
1087 sectioned view using Imaris software (Bitplane). Scale bars: 5 μm.
1088
1089 **Fig. S4: Amino acid comparison between zebrafish, mouse, and human MAK.**
1090 Amino acid sequences of zebrafish, mouse and human MAK proteins are aligned using
1091 Clustal Omega. Grey shading indicates sequence mismatches. The kinase domain is indicated
1092 by an underline. The bottom table shows the percentage of amino acid identity in the full
1093 length protein, the kinase domain, and the C-terminal domain.
1094
1095 **Fig. S5 Measurement of ONL thickness, rod cell number, and the fraction of zpr1-**
1096 **positive area in total retinal area.**

1097 (A) Images with retinas were straightened with Image J (Fuji). Straightened images were
1098 divided into 10 equal areas (A) with 9 deciles (D) between adjacent areas. The thickness
1099 of the ONL was measured at the deciles and cell numbers were counted in each area.
1100 (B) Cryosections labeled with zpr1 antibody were scanned under a laser-scanning microscope
1101 (LSM510; Carl Zeiss, FV3000; Olympus). First, a one-section image containing the
1102 central retina per eye was selected from each individual sample. Using the "split channel"
1103 command of Image J (Fuji), confocal scanning RGB color images were split into either
1104 R, G or B channel. Only the zpr1 channel (green channel in this figure) is used to draw
1105 the outline of the total retinal area. Next, using the "threshold" command of Image J (Fuji),
1106 we converted zpr1-positive and -negative areas to a binary scale, 1 and 0, respectively.
1107 The number of pixels corresponding to 1 or 0 within the neural retina was determined.
1108 Using the "measurement" command of Image J (Fuji), the percentage of zpr1-positive
1109 areas relative to the total retinal area was calculated as the percentage of the number of 1
1110 pixels relative to the number of 0+1 pixels. Means and standard deviations were
1111 calculated from data obtained for 2-5 sections from more than two embryos.

1112

1113 **References**

1114

1115 **Alfinito, P. D. and Townes-Anderson, E.** (2002). Activation of mislocalized opsin kills
1116 rod cells: a novel mechanism for rod cell death in retinal disease. *Proc Natl Acad Sci U S A*
1117 **99**, 5655-5660.

1118 **Athanasiou, D., Aguila, M., Bellingham, J., Li, W., McCulley, C., Reeves, P. J. and**
1119 **Cheetham, M. E.** (2018). The molecular and cellular basis of rhodopsin retinitis
1120 pigmentosa reveals potential strategies for therapy. *Prog Retin Eye Res* **62**, 1-23.

1121 **Bachmann-Gagescu, R. and Neuhauss, S. C.** (2019). The photoreceptor cilium and its
1122 diseases. *Curr Opin Genet Dev* **56**, 22-33.

1123 **Bachmann-Gagescu, R., Phelps, I. G., Stearns, G., Link, B. A., Brockerhoff, S. E.,**
1124 **Moens, C. B. and Doherty, D.** (2011). The ciliopathy gene cc2d2a controls zebrafish
1125 photoreceptor outer segment development through a role in Rab8-dependent vesicle
1126 trafficking. *Hum Mol Genet* **20**, 4041-4055.

1127 **Baehr, W., Hanke-Gogokhia, C., Sharif, A., Reed, M., Dahl, T., Frederick, J. M. and**
1128 **Ying, G.** (2019). Insights into photoreceptor ciliogenesis revealed by animal models. *Prog*
1129 *Retin Eye Res* **71**, 26-56.

1130 **Bahadori, R., Huber, M., Rinner, O., Seeliger, M. W., Geiger-Rudolph, S., Geisler, R.**
1131 **and Neuhauss, S. C.** (2003). Retinal function and morphology in two zebrafish models of
1132 oculo-renal syndromes. *Eur J Neurosci* **18**, 1377-1386.

1133 **Blackshaw, S., Harpavat, S., Trimarchi, J., Cai, L., Huang, H., Kuo, W. P., Weber, G.,**
1134 **Lee, K., Fraioli, R. E., Cho, S. H., et al.** (2004). Genomic analysis of mouse retinal
1135 development. *PLoS Biol* **2**, E247.

1136 **Borovina, A., Superina, S., Voskas, D. and Ciruna, B.** (2010). Vangl2 directs the
1137 posterior tilting and asymmetric localization of motile primary cilia. *Nat Cell Biol* **12**, 407-
1138 412.

1139 **Breslow, D. K. and Holland, A. J.** (2019). Mechanism and Regulation of Centriole and
1140 Cilium Biogenesis. *Annu Rev Biochem* **88**, 691-724.

1141 **Brouhard, G. J. and Rice, L. M.** (2018). Microtubule dynamics: an interplay of
1142 biochemistry and mechanics. *Nat Rev Mol Cell Biol* **19**, 451-463.

1143 **Chaya, T., Omori, Y., Kuwahara, R. and Furukawa, T.** (2014). ICK is essential for cell
1144 type-specific ciliogenesis and the regulation of ciliary transport. *EMBO J* **33**, 1227-1242.

1145 **Chen, H. Y., Kelley, R. A., Li, T. and Swaroop, A.** (2021). Primary cilia biogenesis and
1146 associated retinal ciliopathies. *Semin Cell Dev Biol* **110**, 70-88.

1147 **Chen, T., Wu, D., Moskaluk, C. A. and Fu, Z.** (2013). Distinct expression patterns of
1148 ICK/MAK/MOK protein kinases in the intestine implicate functional diversity. *PLoS One*
1149 **8**, e79359.

1150 **Cideciyan, A. V., Aleman, T. S., Jacobson, S. G., Khanna, H., Sumaroka, A., Aguirre,**
1151 **G. K., Schwartz, S. B., Windsor, E. A., He, S., Chang, B., et al.** (2007). Centrosomal-
1152 ciliary gene CEP290/NPHP6 mutations result in blindness with unexpected sparing of
1153 photoreceptors and visual brain: implications for therapy of Leber congenital amaurosis.
1154 *Hum Mutat* **28**, 1074-1083.

1155 **D'Orazi, F. D., Suzuki, S. C., Darling, N., Wong, R. O. and Yoshimatsu, T.** (2020).
1156 Conditional and biased regeneration of cone photoreceptor types in the zebrafish retina. *J*
1157 *Comp Neurol* **528**, 2816-2830.

1158 **Davis, E. S., E.; Rahmouni, K.; Nishimura, D. Y.; Mullins, R. F.; Agassandian, K.;**
1159 **Philp, A. R.; Searby, C. C.; Andrews, M. P.; Thompson, S.; Berry, C. J.; Thedens, D.**

1160 **R.; Yang, B., Weiss; R. M.; Cassell, M. D.; Stone, E. M.; Sheffield, V. C.** (2007). A
1161 knockin mouse model of the Bardet-Biedl syndrome 1 M390R mutation has cilia defects,
1162 ventriculomegaly, retinopathy, and obesity. *Proc Natl Acad Sci U S A*
1163 **104**, 19422-19427.

1164 **den Hollander, A. I., Koenekoop, R. K., Yzer, S., Lopez, I., Arends, M. L., Voesenek,**
1165 **K. E., Zonneveld, M. N., Strom, T. M., Meitinger, T., Brunner, H. G., et al.** (2006).
1166 Mutations in the CEP290 (NPHP6) gene are a frequent cause of Leber congenital
1167 amaurosis. *Am J Hum Genet* **79**, 556-561.

1168 **Doerre, G. and Malicki, J.** (2002). Genetic analysis of photoreceptor cell development in
1169 the zebrafish retina. *Mech Dev* **110**, 125-138.

1170 **Duldulao, N. A., Lee, S. and Sun, Z.** (2009). Cilia localization is essential for in vivo
1171 functions of the Joubert syndrome protein Arl13b/Scorpion. *Development* **136**, 4033-4042.

1172 **Essner, J. J., Amack, J. D., Nyholm, M. K., Harris, E. B. and Yost, H. J.** (2005).
1173 Kupffer's vesicle is a ciliated organ of asymmetry in the zebrafish embryo that initiates left-
1174 right development of the brain, heart and gut. *Development* **132**, 1247-1260.

1175 **Fain, G. L., Hardie, R. and Laughlin, S. B.** (2010). Phototransduction and the evolution
1176 of photoreceptors. *Curr Biol* **20**, R114-124.

1177 **Gao J., C. K., Nusinowitz Steven, Liu Qin, Bei Di, Atkins Karen, Azimi Asif, Daiger**
1178 **Stephen P. , Farber Debora B., Heckenlively John R., Pierce Eric A., Sullivan Lori S. ,**
1179 **and Zuo Jian** (2002). Progressive photoreceptor degeneration, outer segment dysplasia,
1180 and rhodopsin mislocalization in mice with targeted disruption of the retinitis pigmentosa-1
1181 (Rp1) gene. *The Proceedings of the National Academy of Sciences* **99**, 5698-5703.

1182 **Gao, P., Qin, Y., Qu, Z., Huang, Y., Liu, X., Li, J., Liu, F. and Liu, M.** (2022). The Zpr-
1183 3 antibody recognizes the 320-354 region of Rho and labels both rods and green cones in
1184 zebrafish. *biorxiv*.

1185 **Ge, R., Cao, M., Chen, M., Liu, M. and Xie, S.** (2022). Cytoskeletal networks in primary
1186 cilia: Current knowledge and perspectives. *J Cell Physiol* **237**, 3975-3983.

1187 **Gorden, N. T., Arts, H. H., Parisi, M. A., Coene, K. L., Letteboer, S. J., van Beersum,**
1188 **S. E., Mans, D. A., Hikida, A., Eckert, M., Knutzen, D., et al.** (2008). CC2D2A is
1189 mutated in Joubert syndrome and interacts with the ciliopathy-associated basal body protein
1190 CEP290. *Am J Hum Genet* **83**, 559-571.

1191 **Gray, R. S., Gonzalez, R., Ackerman, S. D., Minowa, R., Griest, J. F., Bayrak, M. N.,**
1192 **Troutwine, B., Canter, S., Monk, K. R., Sepich, D. S., et al.** (2021). Postembryonic
1193 screen for mutations affecting spine development in zebrafish. *Dev Biol* **471**, 18-33.

1194 **Gulati, S. and Palczewski, K.** (2023). Structural view of G protein-coupled receptor
1195 signaling in the retinal rod outer segment. *Trends Biochem Sci* **48**, 172-186.

1196 **Iribarne, M., Hyde, D. R. and Masai, I.** (2019). TNFalpha Induces Muller Glia to
1197 Transition From Non-proliferative Gliosis to a Regenerative Response in Mutant Zebrafish
1198 Presenting Chronic Photoreceptor Degeneration. *Front Cell Dev Biol* **7**, 296.

1199 **Jia, D., Gao, P., Lv, Y., Huang, Y., Reilly, J., Sun, K., Han, Y., Hu, H., Chen, X.,**
1200 **Zhang, Z., et al.** (2022). Tulp1 deficiency causes early-onset retinal degeneration through
1201 affecting ciliogenesis and activating ferroptosis in zebrafish. *Cell Death Dis* **13**, 962.

1202 **Kakakhel, M., Tebbe, L., Makia, M. S., Conley, S. M., Sherry, D. M., Al-Ubaidi, M. R.**
1203 **and Naash, M. I.** (2020). Syntaxin 3 is essential for photoreceptor outer segment protein
1204 trafficking and survival. *Proc Natl Acad Sci U S A* **117**, 20615-20624.

1205 **Karan, S., Zhang, H., Li, S., Frederick, J. M. and Baehr, W.** (2008). A model for
1206 transport of membrane-associated phototransduction polypeptides in rod and cone
1207 photoreceptor inner segments. *Vision Res* **48**, 442-452.

1208 **Klena, N. and Pigino, G.** (2022). Structural Biology of Cilia and Intraflagellar Transport.
1209 *Annu Rev Cell Dev Biol* **38**, 103-123.

1210 **Knapik, E. W., Goodman, A., Ekker, M., Chevrette, M., Delgado, J., Neuhauss, S.,**
1211 **Shimoda, N., Driever, W., Fishman, M. C. and Jacob, H. J.** (1998). A microsatellite
1212 genetic linkage map for zebrafish (Danio rerio). *Nat Genet* **18**, 338-343.

1213 **Krock, B. L. and Perkins, B. D.** (2008). The intraflagellar transport protein IFT57 is
1214 required for cilia maintenance and regulates IFT-particle-kinesin-II dissociation in
1215 vertebrate photoreceptors. *J Cell Sci* **121**, 1907-1915.

1216 **Kwan, K. M., Fujimoto, E., Grabher, C., Mangum, B. D., Hardy, M. E., Campbell, D.**
1217 **S., Parant, J. M., Yost, H. J., Kanki, J. P. and Chien, C. B.** (2007). The Tol2kit: a
1218 multisite gateway-based construction kit for Tol2 transposon transgenesis constructs. *Dev*
1219 *Dyn* **236**, 3088-3099.

1220 **Larison, K. D. and Bremiller, R.** (1990). Early onset of phenotype and cell patterning in
1221 the embryonic zebrafish retina. *Development* **109**, 567-576.

1222 **Latour, B. L., Van De Weghe, J. C., Rusterholz, T. D., Letteboer, S. J., Gomez, A.,**
1223 **Shaheen, R., Gesemann, M., Karamzade, A., Asadollahi, M., Barroso-Gil, M., et al.**
1224 (2020). Dysfunction of the ciliary ARMC9/TOGARAM1 protein module causes Joubert
1225 syndrome. *J Clin Invest* **130**, 4423-4439.

1226 **Lee, S. J., Emery, D., Vukmanic, E., Wang, Y., Lu, X., Wang, W., Fortuny, E., James,**
1227 **R., Kaplan, H. J., Liu, Y., et al.** (2023). Metabolic transcriptomics dictate responses of
1228 cone photoreceptors to retinitis pigmentosa. *Cell Rep* **42**, 113054.

1229 **Liu, Q., Zuo, J. and Pierce, E. A.** (2004). The retinitis pigmentosa 1 protein is a
1230 photoreceptor microtubule-associated protein. *J Neurosci* **24**, 6427-6436.

1231 **Lopes, V. J., D.; Khanobdee, K.; Song, X.; Chen, B.; Nusinowitz, S.; Williams, DS.**
1232 (2010). Dysfunction of heterotrimeric kinesin-2 in rod photoreceptor cells and the role of
1233 opsin mislocalization in rapid cell death. *Mol Biol Cell*. **21**, 4076-4088.

1234 **Ma, A. H., Xia, L., Desai, S. J., Boucher, D. L., Guan, Y., Shih, H. M., Shi, X. B.,**
1235 **deVere White, R. W., Chen, H. W., Tepper, C. G., et al.** (2006). Male germ cell-
1236 associated kinase, a male-specific kinase regulated by androgen, is a coactivator of
1237 androgen receptor in prostate cancer cells. *Cancer Res* **66**, 8439-8447.

1238 **Malicki, J. J. and Johnson, C. A.** (2017). The Cilium: Cellular Antenna and Central
1239 Processing Unit. *Trends Cell Biol* **27**, 126-140.

1240 **Masek, M., Etard, C., Hofmann, C., Hulsmeier, A. J., Zang, J., Takamiya, M.,**
1241 **Gesemann, M., Neuhauss, S. C. F., Hornemann, T., Strahle, U., et al.** (2022). Loss of
1242 the Bardet-Biedl protein Bbs1 alters photoreceptor outer segment protein and lipid
1243 composition. *Nat Commun* **13**, 1282.

1244 **Matsushime, H., Jinno, A., Takagi, N. and Shibuya, M.** (1990). A novel mammalian
1245 protein kinase gene (mak) is highly expressed in testicular germ cells at and after meiosis.
1246 *Molecular and cellular biology* **10**, 2261-2268.

1247 **Mercer, A. J. and Thoreson, W. B.** (2011). The dynamic architecture of photoreceptor
1248 ribbon synapses: cytoskeletal, extracellular matrix, and intramembrane proteins. *Vis*
1249 *Neurosci* **28**, 453-471.

1250 **Messchaert, M., Dona, M., Broekman, S., Peters, T. A., Corral-Serrano, J. C.,**
1251 **Slijkerman, R. W. N., van Wijk, E. and Collin, R. W. J.** (2018). Eyes shut homolog is
1252 important for the maintenance of photoreceptor morphology and visual function in
1253 zebrafish. *PLoS One* **13**, e0200789.

1254 **Miyata, Y. and Nishida, E.** (1999). Distantly related cousins of MAP kinase: biochemical
1255 properties and possible physiological functions. *Biochem Biophys Res Commun* **266**, 291-
1256 295.

1257 **Muto, A., Orger, M. B., Wehman, A. M., Smear, M. C., Kay, J. N., Page-McCaw, P.**
1258 **S., Gahtan, E., Xiao, T., Nevin, L. M., Gosse, N. J., et al.** (2005). Forward genetic
1259 analysis of visual behavior in zebrafish. *PLoS Genet* **1**, e66.

1260 **Nakamura, K., Noguchi, T., Takahara, M., Omori, Y., Furukawa, T., Katoh, Y. and**
1261 **Nakayama, K.** (2020). Anterograde trafficking of ciliary MAP kinase-like ICK/CILK1 by
1262 the intraflagellar transport machinery is required for intraciliary retrograde protein
1263 trafficking. *J Biol Chem* **295**, 13363-13376.

1264 **Nakayama, K. and Katoh, Y.** (2018). Ciliary protein trafficking mediated by IFT and
1265 BBSome complexes with the aid of kinesin-2 and dynein-2 motors. *J Biochem* **163**, 155-
1266 164.

1267 **Nishiwaki, Y. and Masai, I.** (2020). beta-SNAP activity in the outer segment growth
1268 period is critical for preventing BNip1-dependent apoptosis in zebrafish photoreceptors. *Sci*
1269 *Rep* **10**, 17379.

1270 **Nishiwaki, Y., Yoshizawa, A., Kojima, Y., Oguri, E., Nakamura, S., Suzuki, S., Yuasa-**
1271 **Kawada, J., Kinoshita-Kawada, M., Mochizuki, T. and Masai, I.** (2013). The BH3-only
1272 SNARE BNip1 mediates photoreceptor apoptosis in response to vesicular fusion defects.
1273 *Dev Cell* **25**, 374-387.

1274 **Oberhammer, F. A., Hochegger, K., Froschl, G., Tiefenbacher, R. and Pavelka, M.**
1275 (1994). Chromatin condensation during apoptosis is accompanied by degradation of lamin
1276 A+B, without enhanced activation of cdc2 kinase. *J Cell Biol* **126**, 827-837.

1277 **Oel, A. P., Neil, G. J., Dong, E. M., Balay, S. D., Collett, K. and Allison, W. T.** (2020).
1278 Nrl Is Dispensable for Specification of Rod Photoreceptors in Adult Zebrafish Despite Its
1279 Deeply Conserved Requirement Earlier in Ontogeny. *iScience* **23**, 101805.

1280 **Omori, Y., Chaya, T., Katoh, K., Kajimura, N., Sato, S., Muraoka, K., Ueno, S.,**
1281 **Koyasu, T., Kondo, M. and Furukawa, T.** (2010). Negative regulation of ciliary length
1282 by ciliary male germ cell-associated kinase (Mak) is required for retinal photoreceptor
1283 survival. *Proc Natl Acad Sci U S A* **107**, 22671-22676.

1284 **Omori, Y., Zhao, C., Saras, A., Mukhopadhyay, S., Kim, W., Furukawa, T., Sengupta,**
1285 **P., Veraksa, A. and Malicki, J.** (2008). Elipsa is an early determinant of ciliogenesis that
1286 links the IFT particle to membrane-associated small GTPase Rab8. *Nat Cell Biol* **10**, 437-
1287 444.

1288 **Ozgul, R. K., Siemiatkowska, A. M., Yucel, D., Myers, C. A., Collin, R. W.,**
1289 **Zonneveld, M. N., Beryozkin, A., Banin, E., Hoyng, C. B., van den Born, L. I., et al.**
1290 (2011). Exome sequencing and cis-regulatory mapping identify mutations in MAK, a gene
1291 encoding a regulator of ciliary length, as a cause of retinitis pigmentosa. *Am J Hum Genet*
1292 **89**, 253-264.

1293 **Park, K. and Leroux, M. R.** (2022). Composition, organization and mechanisms of the
1294 transition zone, a gate for the cilium. *EMBO Rep* **23**, e55420.

1295 **Rao, K. N., Li, L., Anand, M. and Khanna, H.** (2015). Ablation of retinal ciliopathy
1296 protein RPGR results in altered photoreceptor ciliary composition. *Sci Rep* **5**, 11137.

1297 **Reynolds, E.** (1963). The use of lead citrate at high pH as an electron-opaque stain in
1298 electron microscopy. *The Journal of cell biology* **17**, 208-212.

1299 **Rohrer, B., Lohr, H. R., Humphries, P., Redmond, T. M., Seeliger, M. W. and**
1300 **Crouch, R. K.** (2005). Cone opsin mislocalization in Rpe65-/- mice: a defect that can be
1301 corrected by 11-cis retinal. *Invest Ophthalmol Vis Sci* **46**, 3876-3882.

1302 **Shimoda, N., Knapik, E. W., Ziniti, J., Sim, C., Yamada, E., Kaplan, S., Jackson, D.,**
1303 **de Sauvage, F., Jacob, H. and Fishman, M. C.** (1999). Zebrafish genetic map with 2000
1304 microsatellite markers. *Genomics* **58**, 219-232.

1305 **Song, P., Dudinsky, L., Fogerty, J., Gaivin, R. and Perkins, B. D.** (2016). Arl13b
1306 Interacts With Vangl2 to Regulate Cilia and Photoreceptor Outer Segment Length in
1307 Zebrafish. *Invest Ophthalmol Vis Sci* **57**, 4517-4526.

1308 **Stone, E. M., Luo, X., Héon, E., Lam, B. L., Weleber, R. G., Halder, J. A., Affatigato,**
1309 **L. M., Goldberg, J. B., Sumaroka, A., Schwartz, S. B., et al.** (2011). Autosomal
1310 Recessive Retinitis Pigmentosa Caused by Mutations in theMAKGene. *Investigative*
1311 *Opthalmology & Visual Science* **52**.

1312 **Sukumaran, S. and Perkins, B. D.** (2009). Early defects in photoreceptor outer segment
1313 morphogenesis in zebrafish ift57, ift88 and ift172 Intraflagellar Transport mutants. *Vision*
1314 *Res* **49**, 479-489.

1315 **Suzuki, S. C., Bleckert, A., Williams, P. R., Takechi, M., Kawamura, S. and Wong, R.**
1316 **O.** (2013). Cone photoreceptor types in zebrafish are generated by symmetric terminal
1317 divisions of dedicated precursors. *Proc Natl Acad Sci U S A* **110**, 15109-15114.

1318 **Thisse, C. and Thisse, B.** (2008). High-resolution in situ hybridization to whole-mount
1319 zebrafish embryos. *Nat Protoc* **3**, 59-69.

1320 **Tian, X., Zhao, H. and Zhou, J.** (2023). Organization, functions, and mechanisms of the
1321 BBSome in development, ciliopathies, and beyond. *Elife* **12**.

1322 **Tsujikawa, M. and Malicki, J.** (2004). Intraflagellar transport genes are essential for
1323 differentiation and survival of vertebrate sensory neurons. *Neuron* **42**, 703-716.

1324 **Urasaki, A., Morvan, G. and Kawakami, K.** (2006). Functional dissection of the Tol2
1325 transposable element identified the minimal cis-sequence and a highly repetitive sequence
1326 in the subterminal region essential for transposition. *Genetics* **174**, 639-649.

1327 **Vihtelic, T. S., Doro, C. J. and Hyde, D. R.** (1999). Cloning and characterization of six
1328 zebrafish photoreceptor opsin cDNAs and immunolocalization of their corresponding
1329 proteins. *Vis Neurosci* **16**, 571-585.

1330 **Wang, J. and Deretic, D.** (2014). Molecular complexes that direct rhodopsin transport to
1331 primary cilia. *Prog Retin Eye Res* **38**, 1-19.

1332 **Wang, J., Thomas, H. R., Thompson, R. G., Waldrep, S. C., Fogerty, J., Song, P., Li,**
1333 **Z., Ma, Y., Santra, P., Hoover, J. D., et al.** (2022). Variable phenotypes and penetrance
1334 between and within different zebrafish ciliary transition zone mutants. *Dis Model Mech* **15**.

1335 **Wang, L. Y. and Kung, H. J.** (2012). Male germ cell-associated kinase is overexpressed
1336 in prostate cancer cells and causes mitotic defects via deregulation of APC/CCDH1.
1337 *Oncogene* **31**, 2907-2918.

1338 **Westerfield, M.** (2000). *The zebrafish book. A guide for the laboratory use of zebrafish*
1339 *(Danio rerio)*. (4th edn): Univ. of Oregon Press, Eugene.

1340 **Xia, L., Robinson, D., Ma, A. H., Chen, H. C., Wu, F., Qiu, Y. and Kung, H. J.** (2002).
1341 Identification of human male germ cell-associated kinase, a kinase transcriptionally
1342 activated by androgen in prostate cancer cells. *J Biol Chem* **277**, 35422-35433.

1343 **Yin, J., Brocher, J., Linder, B., Hirmer, A., Sundaramurthi, H., Fischer, U. and**
1344 **Winkler, C.** (2012). The 1D4 antibody labels outer segments of long double cone but not
1345 rod photoreceptors in zebrafish. *Invest Ophthalmol Vis Sci* **53**, 4943-4951.

1346 **Yu, H., Guo, P., Xie, X., Wang, Y. and Chen, G.** (2017). Ferroptosis, a new form of cell
1347 death, and its relationships with tumourous diseases. *J Cell Mol Med* **21**, 648-657.

1348 **Zhai, G., Gu, Q., He, J., Lou, Q., Chen, X., Jin, X., Bi, E. and Yin, Z.** (2014). Sept6 is
1349 required for ciliogenesis in Kupffer's vesicle, the pronephros, and the neural tube during
1350 early embryonic development. *Mol Cell Biol* **34**, 1310-1321.

1351 **Zhu, P., Xu, J., Wang, Y. and Zhao, C.** (2021). Loss of Ift74 Leads to Slow
1352 Photoreceptor Degeneration and Ciliogenesis Defects in Zebrafish. *Int J Mol Sci* **22**.

1353 **Zolessi, F. R., Berois, N., Brauer, M. M. and Castillo, E.** (2021). Building the embryo of
1354 Developmental Biology in Uruguay. *Int J Dev Biol* **65**, 71-76.

1355

1356
1357

1358 **Appendix**

1359 **Antibodies**

NAME	SPECIES	SOURCE	USAGE	REMARK
Zpr-1	Mouse mAb	ZIRC	IHC: 1:100	
Zpr-3	Mouse mAb	ZIRC	IHC: 1:100	recognize zebrafish green opsin and rhodopsin (Gao et al., 2022)
Anti-Rhodopsin	Mouse mAb, clone 1D4	Abcam, ab5417	IHC: 1:100	recognize zebrafish red opsin (Yin et al., 2012)
Anti-GFP	Rabbit pAb	Invitrogen, A11122	IHC: 1:100	
Anti-acetylated Tubulin	Mouse mAb, clone 6-11B-1	Sigma Aldrich, T7451	IHC: 1:250	
Anti-EYS	Rabbit pAb	Novus Bio, NBP1-90038	IHC: 1:300	pH 6.0 HIAR
Anti-gamma Tubulin	Mouse mAb, clone GTU88	Sigma Aldrich, T6557	IHC: 1:100	pH 6.0 HIAR
Anti-MAK	Rabbit pAb	Scrum Inc.	WB: 1:1000	custom ab
Anti-MBP	Mouse mAb, clone SKB3	Merck, 05-675	WB: 1:5000	
Anti-phospho-MBP	Mouse mAb, clone P12	Merck, 05-429	WB: 1:10000	
Anti-GST	Mouse mAb, clone B-14	Santa Cruz, sc-138	WB: 1:10000	
Anti-zebrafish rhodopsin	Rabbit pAb	ZFIN: ZDB-ATB-09058-5	IHC: 1:5000	Ref. Vihtelic and Hyde, 1999 (DOI: 10.1017/s0952523899163168)

1360

1361 **Primers**

NAME	SEQUENCE (5’ TO 3’)	REMARK
z23011_Fw	TTGGGGAAAAAGTCTGCTTG	SSLP BSA
z23011_Rev	TCCAACATGTAAAAACCTGACAA	SSLP BSA
mak-N1_Fw	GTGCAAGGTGTGAATTAGAC	SSLP BSA
mak-N1_Rev	AACTTCCCGACTTCTGTAAC	SSLP BSA
mak_Fw3	ACAGTGGGATGGAGTGGCATCCCTT	mak cDNA cloning
mak_Rev3	TTTCCGAGCGTTGAAAGTAGTCC	mak cDNA cloning
mak-I4_Fw	TGATGTTCACCAGCCACACT	pday site sequence
mak-I3_Rev	TCCCAGTTTTGATGTTGCAT	pday site sequence
mak-E5_Fw	CACAAATGCCAAACCAGAGA	pday site sequence

mak-E4_Rev	TGGTGAAGCTAAAGGAGGTGA	pday site sequence
MAK-AR_Fw	AGTGGCCATCgcgAGAATGAAGAG	AR MAK mutagenesis
MAK-AR_Rev	CTCTTCATTCTcgcGATGGCCACT	AR MAK mutagenesis
MAK-ADF_Fw	cttcGTCTCAACACGATGGTATCGAG	ADF MAK mutagenesis
MAK-ADF_Rev	tctgcGTAAGGTGGCCGAGAGCG	ADF MAK mutagenesis
arl13b_Fw	GGAAATGTTCAATCTGATGGCGAACTG	arl13b cDNA cloning
arl13b_Rev	GTGTTAGGAAATGACATCATGAGTATCGC	arl13b cDNA cloning
T3_mak_Fw	CTAATTAACCCTCACTAAAGGATGAACCGTTACACGACACTCAAG	mak in situ probe
mak_T7_Rev	CTTAATACGACTCACTATAGGGTTAACGATGGCTTCCATATT	mak in situ probe
Z13695_Fw	TGTCGTAGGACATGGGGATT	BSA SSLP
Z13695_Rev	TCGCTGCTTCGTTCTCACTA	BSA SSLP

1362
1363

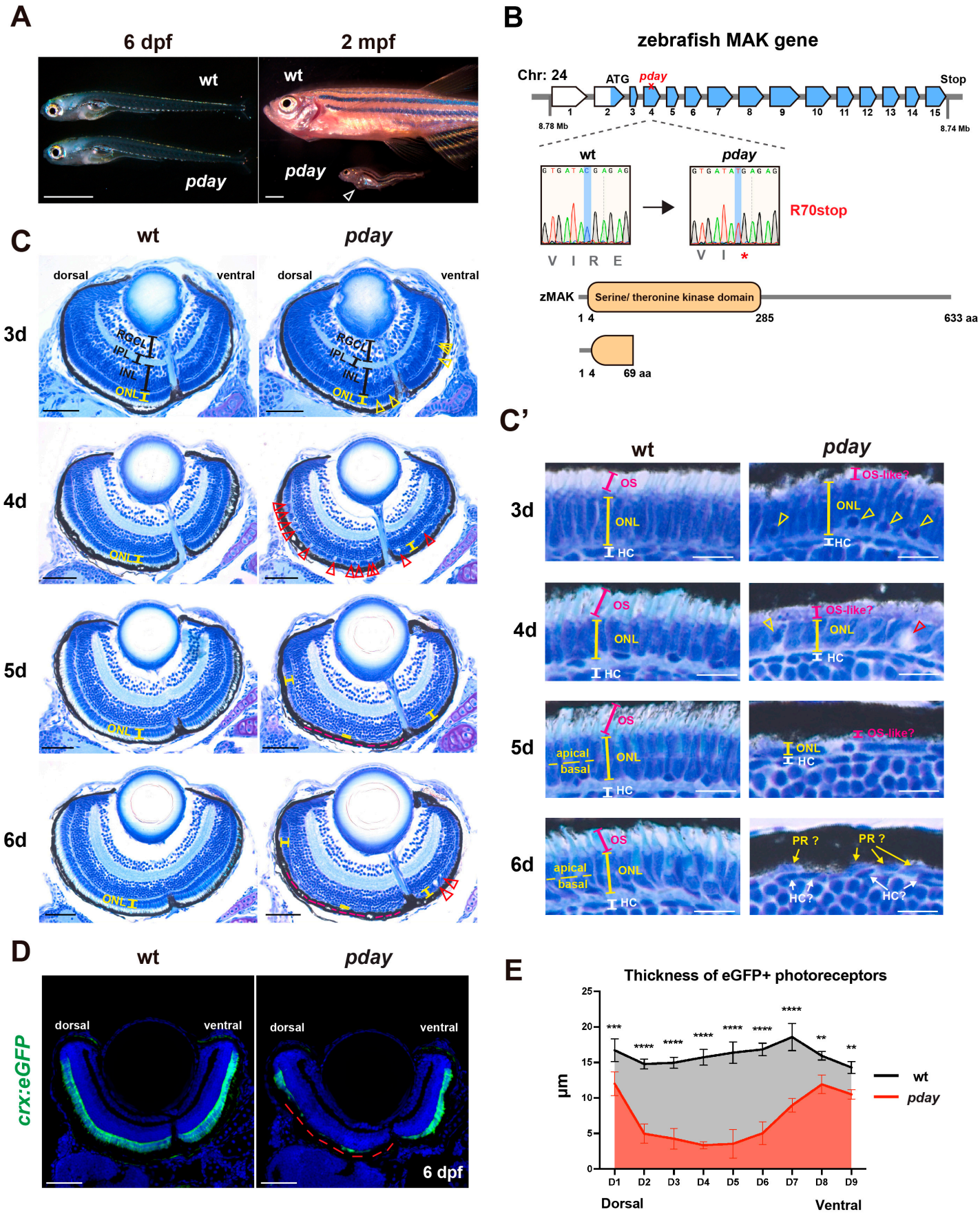
A
6 dpf
2 mpf
wt
pday
B
zebrafish MAK gene
Chr: 24
ATG
pday
Stop
8.78 Mb
8.74 Mb
wt
pday
R70stop
V I R E
V I *
zMAK
Serine/ theronine kinase domain
1 4
285
633 aa
1 4
69 aa
C
wt
pday
dorsal
ventral
3d
4d
5d
6d
RGCL
IPL
INL
ONL
C'
OS
OS-like?
ONL
HC
apical
basal
PR ?
HC?
D
crx:eGFP
6 dpf
E
Thickness of eGFP+ photoreceptors
µm
wt
pday
D1
D2
D3
D4
D5
D6
D7
D8
D9
Dorsal
Ventral

Figure 1

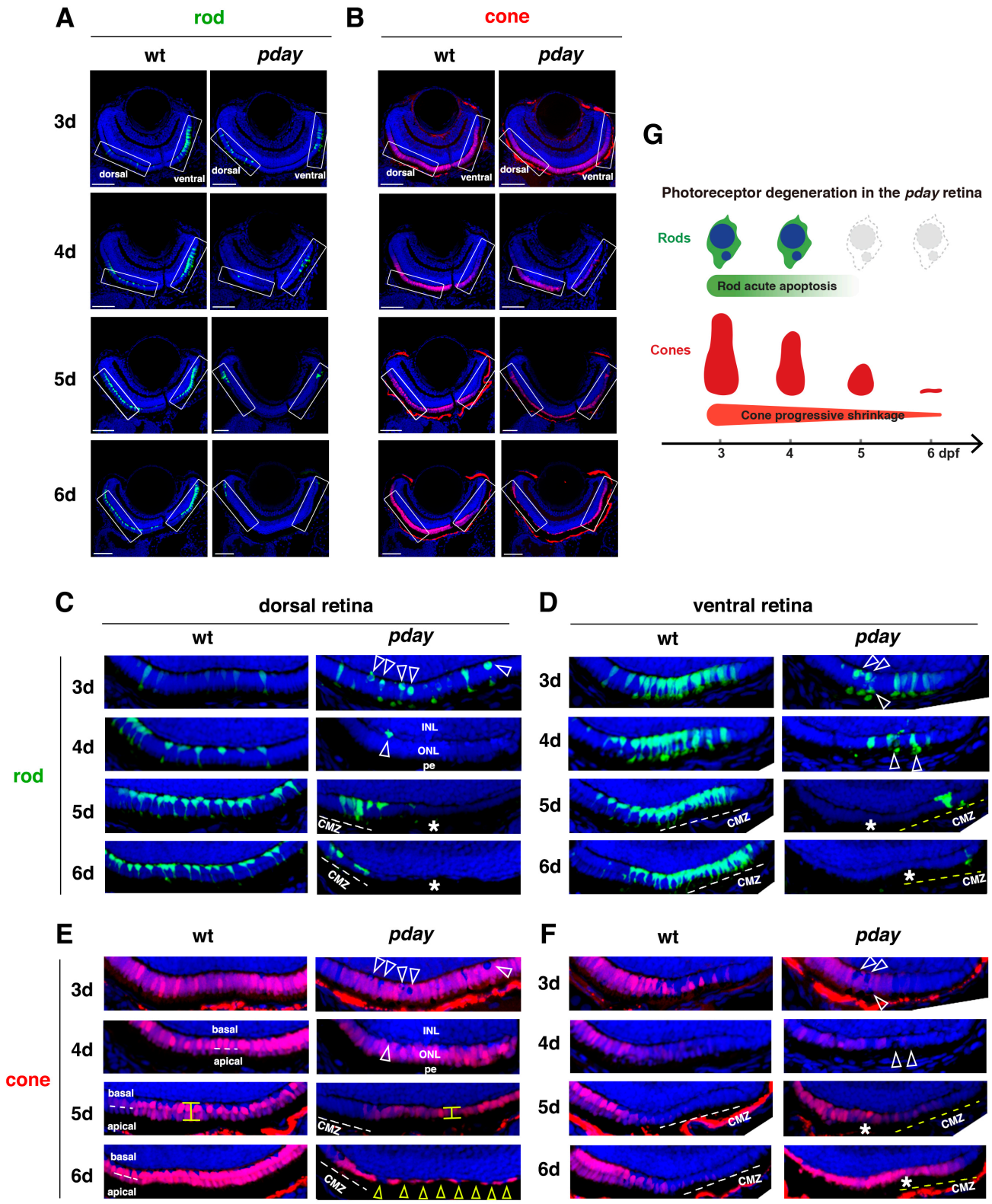
A
rod
wt
pday
3d
4d
5d
6d
dorsal
ventral
B
cone
wt
pday
G
Photoreceptor degeneration in the pday retina
Rods
Rod acute apoptosis
Cones
Cone progressive shrinkage
3
4
5
6 dpf
C
dorsal retina
wt
pday
rod
INL
ONL
pe
CMZ
D
ventral retina
E
cone
basal
apical
F

Figure 2

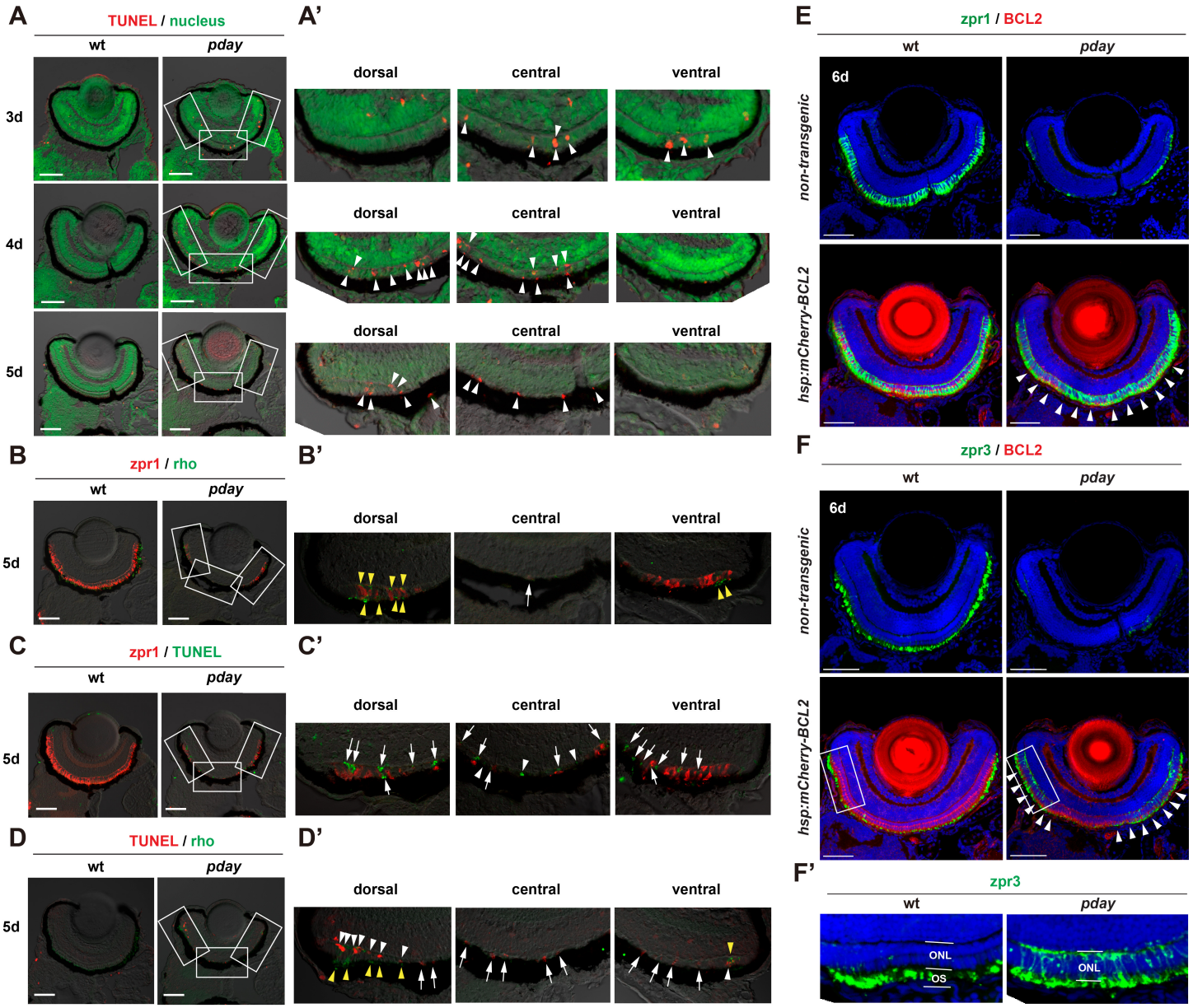
A
TUNEL / nucleus
wt
pday
3d
4d
5d
A'
dorsal
central
ventral
B
zpr1 / rho
B'
C
zpr1 / TUNEL
C'
D
TUNEL / rho
D'
E
zpr1 / BCL2
6d
non-transgenic
hsp:mCherry-BCL2
F
zpr3 / BCL2
F'
zpr3
ONL
OS

Figure 3

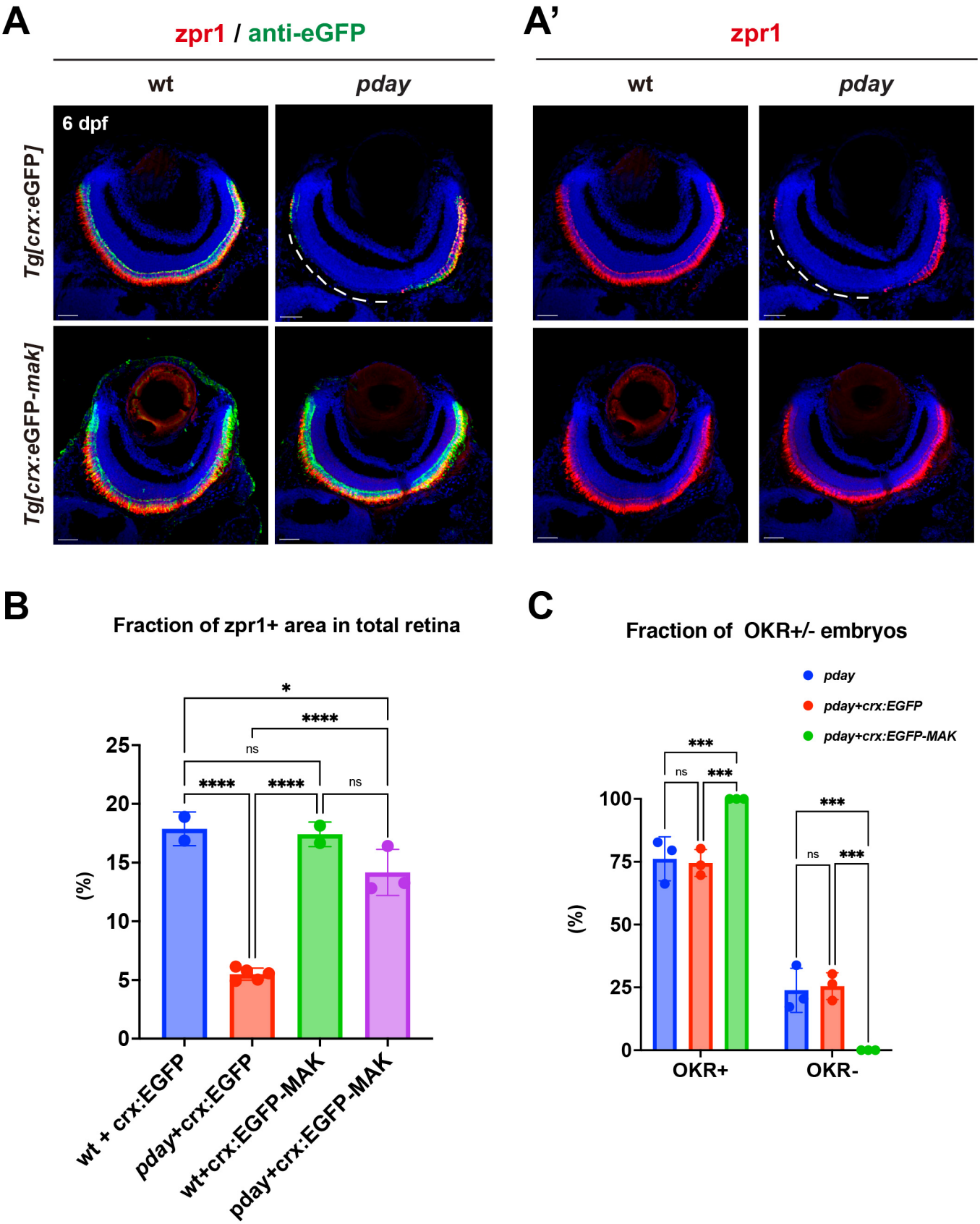
A
zpr1 / anti-eGFP
wt
pday
6 dpf
Tg[crx:eGFP]
Tg[crx:eGFP-mak]
A'
zpr1
wt
pday
B
Fraction of zpr1+ area in total retina
(%)
25
20
15
10
5
0
*
****
ns
****
****
ns
wt + crx:EGFP
pday+crx:EGFP
wt+crx:EGFP-MAK
pday+crx:EGFP-MAK
C
Fraction of OKR+/- embryos
pday
pday+crx:EGFP
pday+crx:EGFP-MAK
(%)
100
75
50
25
0
***
ns
***
***
ns
***
OKR+
OKR-

Figure 4

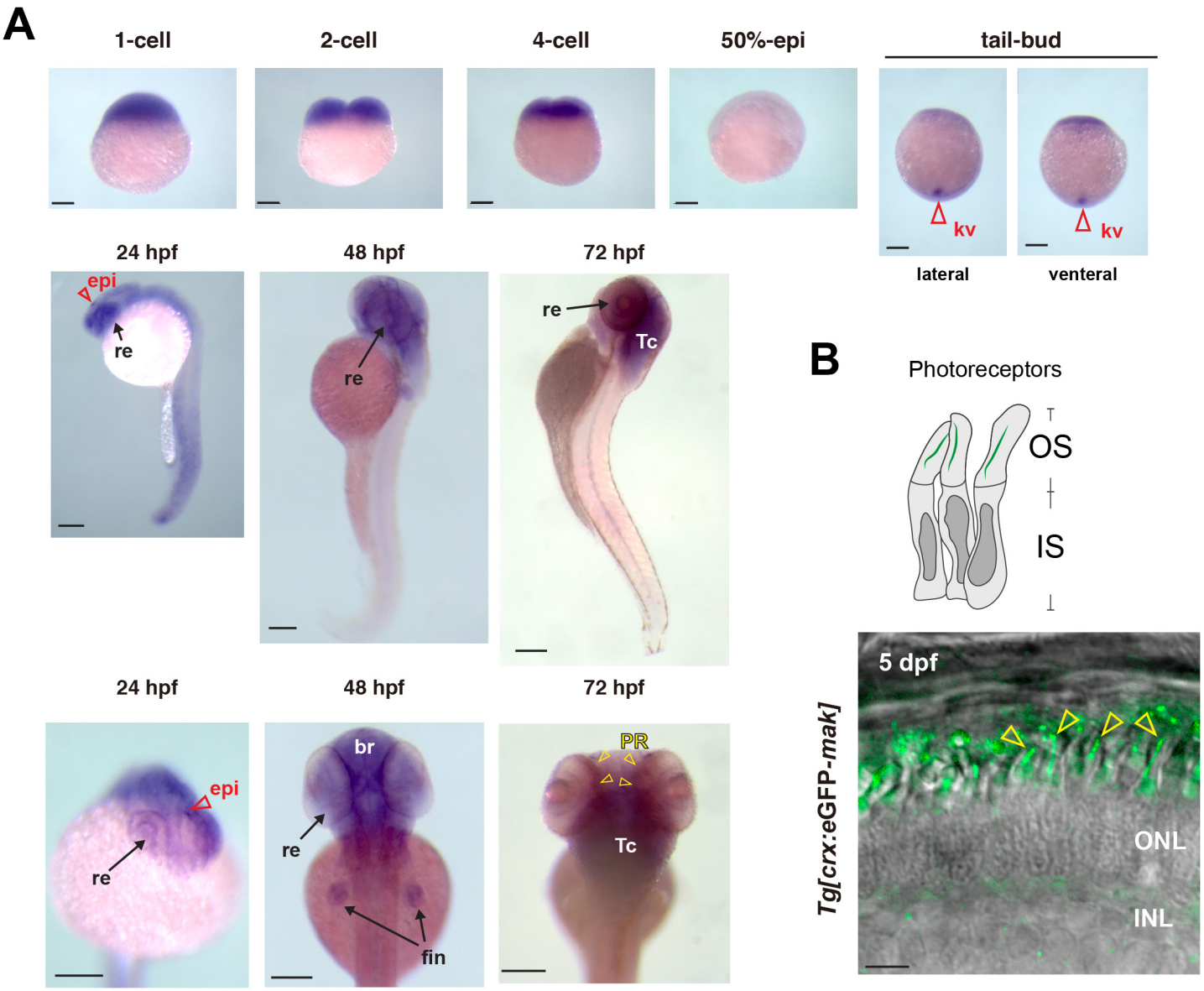
A
1-cell
2-cell
4-cell
50%-epi
tail-bud
kv
kv
lateral
venteral
24 hpf
48 hpf
72 hpf
epi
re
re
re
Tc
24 hpf
48 hpf
72 hpf
epi
re
br
re
fin
PR
Tc
B
Photoreceptors
OS
IS
5 dpf
Tg[crx:eGFP-mak]
ONL
INL

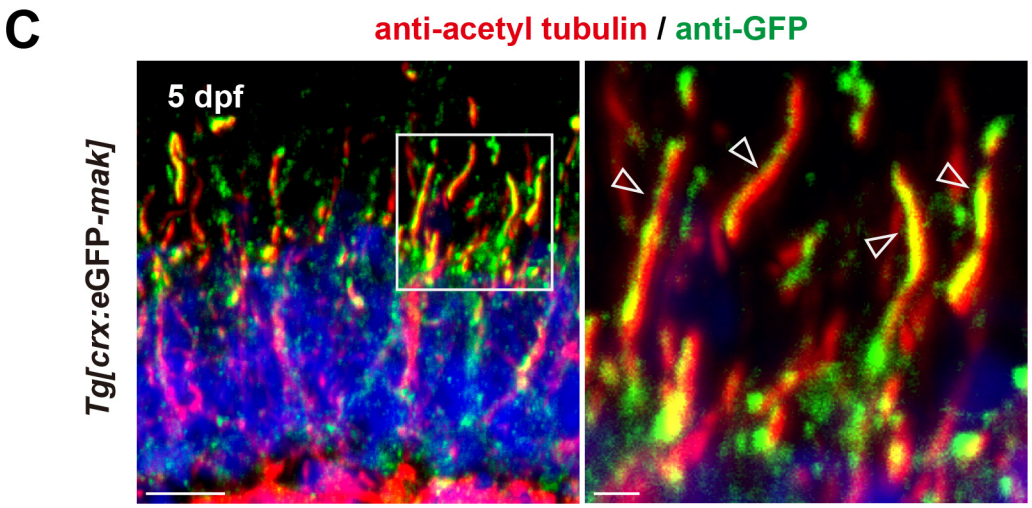
C
anti-acetyl tubulin / anti-GFP
5 dpf
Tg[crx:eGFP-mak]

Figure 5

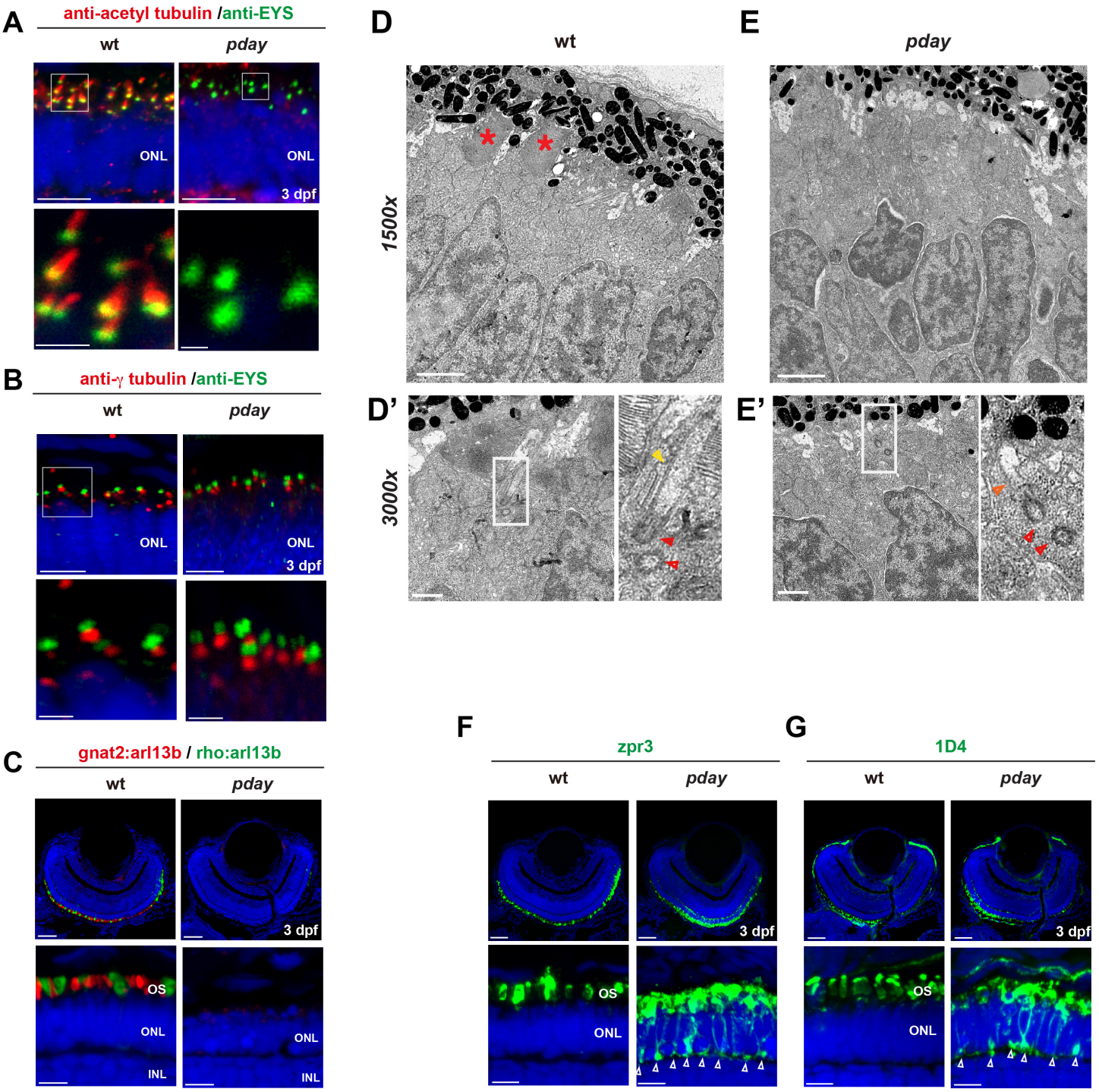
A
anti-acetyl tubulin /anti-EYS
wt
pday
ONL
ONL
3 dpf
B
anti-γ tubulin /anti-EYS
wt
pday
ONL
ONL
3 dpf
C
gnat2:arl13b / rho:arl13b
wt
pday
3 dpf
OS
ONL
INL
ONL
INL
D
wt
1500x
D'
3000x
E
pday
E'
F
zpr3
wt
pday
3 dpf
OS
ONL
G
1D4
wt
pday
3 dpf
OS
ONL

Figure 6

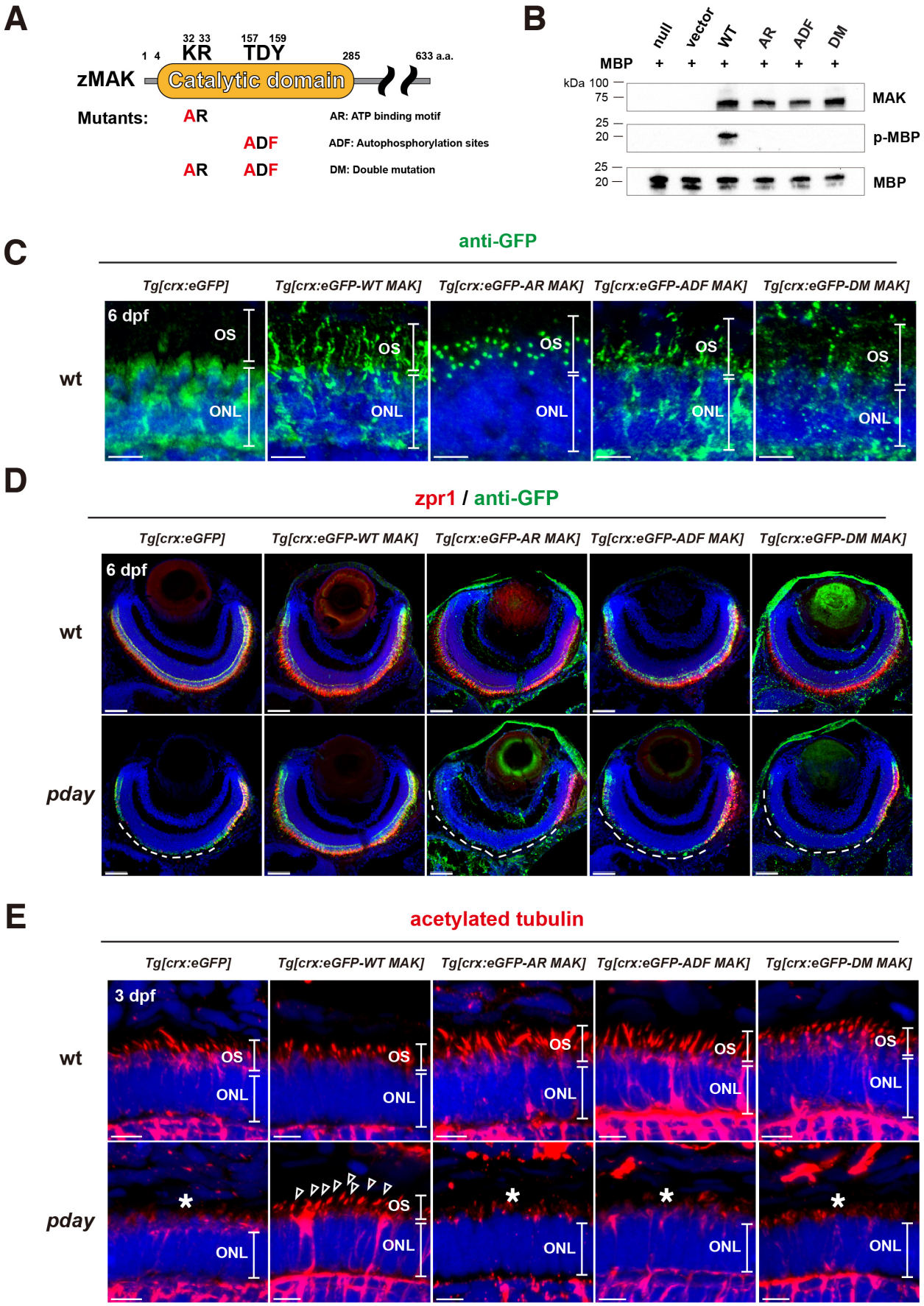
A
32 33
KR
157 159
TDY
1 4
285
633 a.a.
zMAK
Catalytic domain
Mutants:
AR
AR: ATP binding motif
ADF
ADF: Autophosphorylation sites
AR ADF
DM: Double mutation
B
null
vector
WT
AR
ADF
DM
MBP + + + + + +
kDa 100
75
MAK
25
20
p-MBP
25
20
MBP
C
anti-GFP
Tg[crx:eGFP]
Tg[crx:eGFP-WT MAK]
Tg[crx:eGFP-AR MAK]
Tg[crx:eGFP-ADF MAK]
Tg[crx:eGFP-DM MAK]
6 dpf
wt
OS
ONL
D
zpr1 / anti-GFP
Tg[crx:eGFP]
Tg[crx:eGFP-WT MAK]
Tg[crx:eGFP-AR MAK]
Tg[crx:eGFP-ADF MAK]
Tg[crx:eGFP-DM MAK]
6 dpf
wt
pday
E
acetylated tubulin
Tg[crx:eGFP]
Tg[crx:eGFP-WT MAK]
Tg[crx:eGFP-AR MAK]
Tg[crx:eGFP-ADF MAK]
Tg[crx:eGFP-DM MAK]
3 dpf
wt
pday
OS
ONL

Figure 7

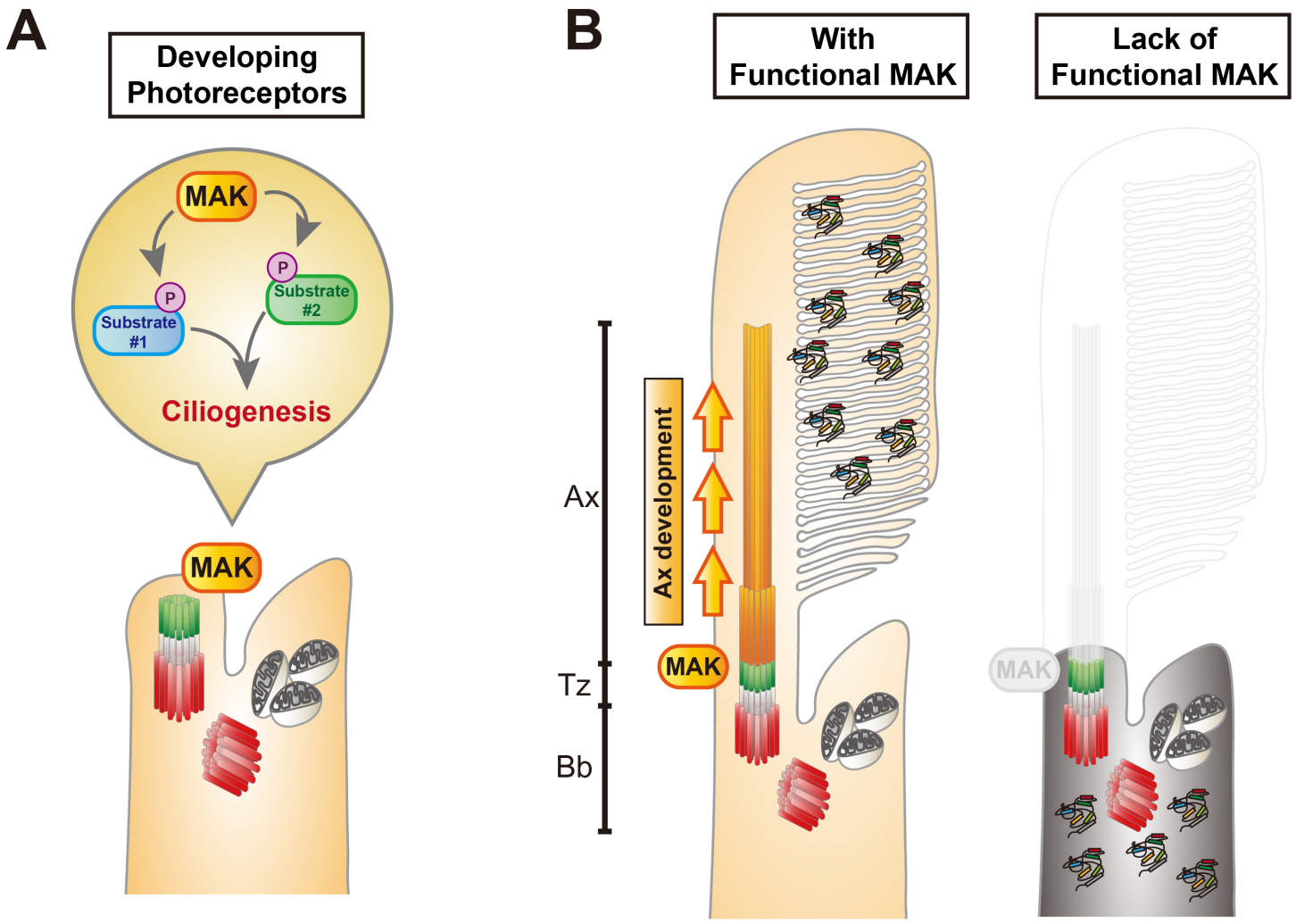
A
Developing Photoreceptors
MAK
P
Substrate #1
P
Substrate #2
Ciliogenesis
MAK
B
With Functional MAK
Lack of Functional MAK
Ax
Tz
Bb
Ax development
MAK
MAK

Figure 8

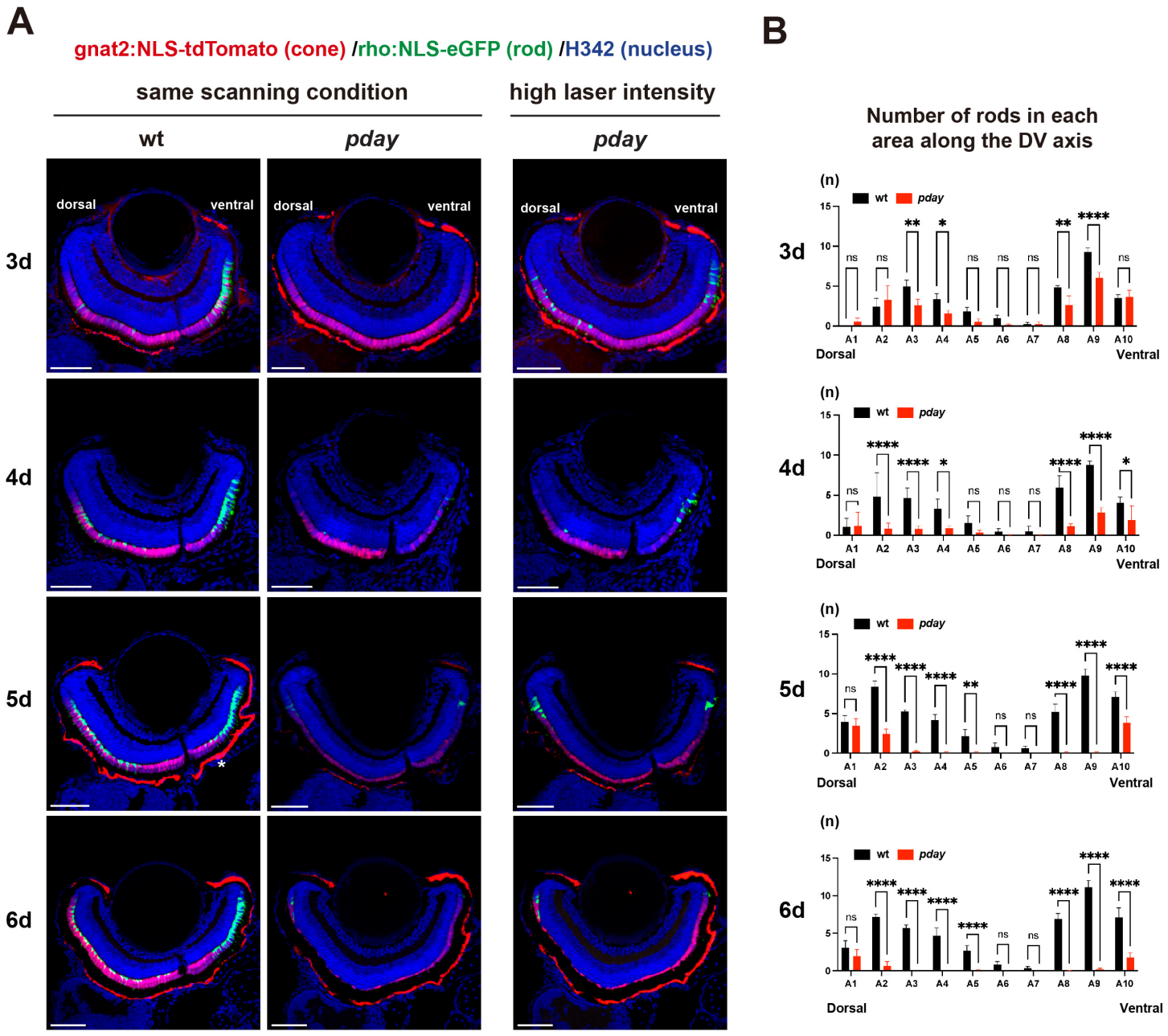
A
gnat2:NLS-tdTomato (cone) /rho:NLS-eGFP (rod) /H342 (nucleus)
same scanning condition
high laser intensity
wt
pday
pday
dorsal
ventral
3d
4d
5d
6d
B
Number of rods in each area along the DV axis
(n)
wt
pday
A1
A2
A3
A4
A5
A6
A7
A8
A9
A10
Dorsal
Ventral

Figure S1

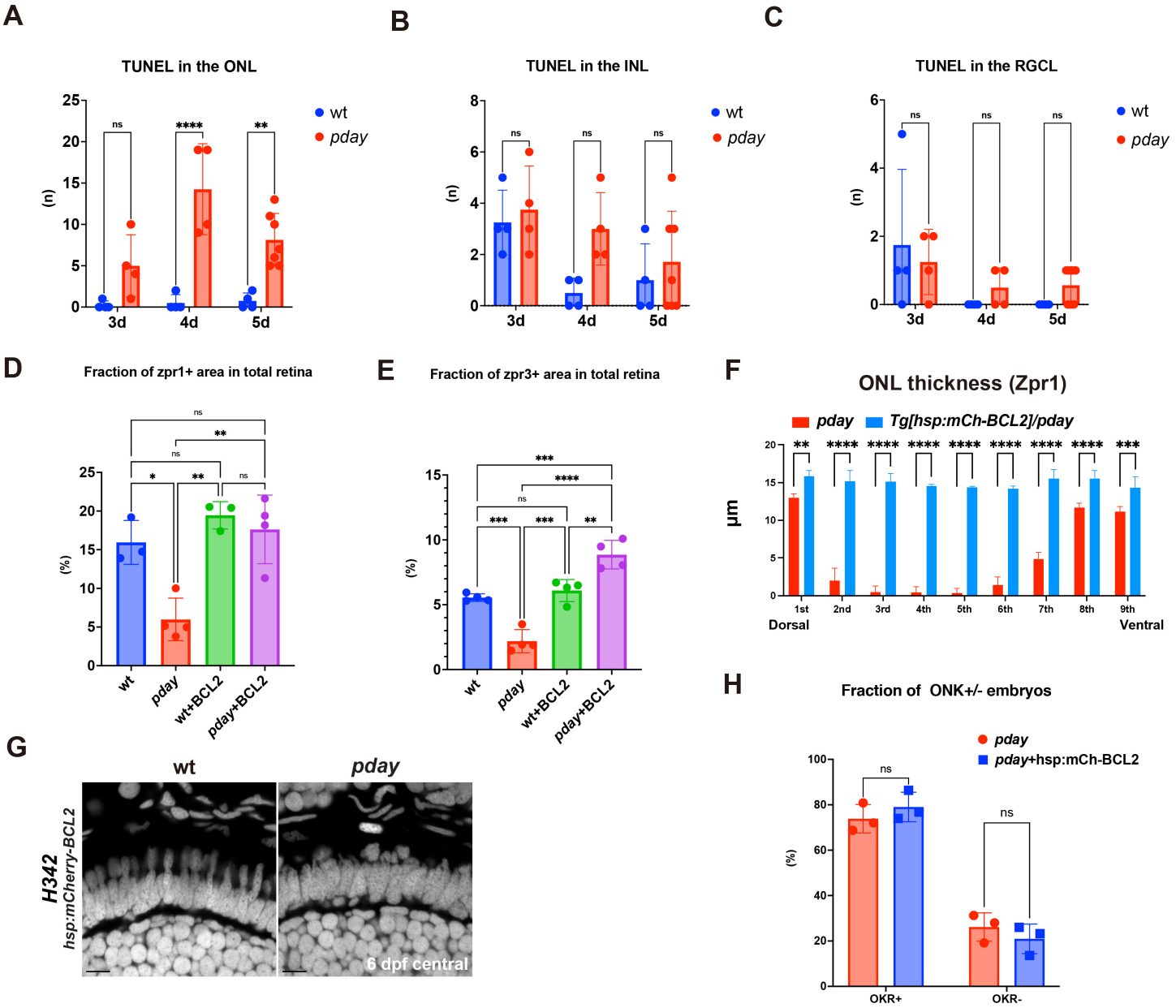
A
TUNEL in the ONL
(n)
wt
pday
ns
****
**
3d
4d
5d
B
TUNEL in the INL
C
TUNEL in the RGCL
D
Fraction of zpr1+ area in total retina
(%)
wt
pday
wt+BCL2
pday+BCL2
E
Fraction of zpr3+ area in total retina
F
ONL thickness (Zpr1)
pday
Tg[hsp:mCh-BCL2]/pday
µm
1st
2nd
3rd
4th
5th
6th
7th
8th
9th
Dorsal
Ventral
G
wt
pday
H342
hsp:mCherry-BCL2
6 dpf central
H
Fraction of ONK+/- embryos
pday+hsp:mCh-BCL2
OKR+
OKR-

Figure S2

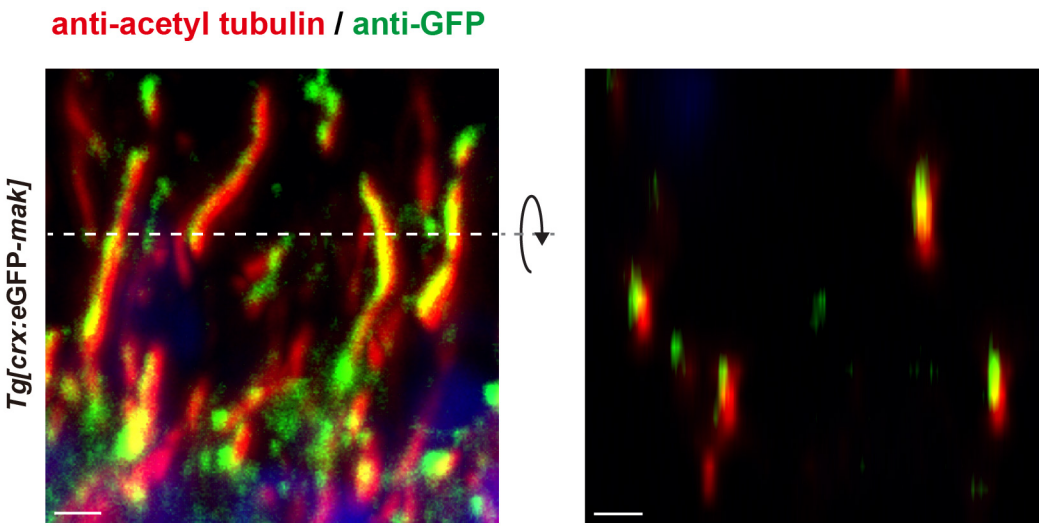

Figure S3

```
                1                                                                                                                                                                                                                                                                                                                                                                                                                                                                                                                                                                                                                                                                                                                                                                                                                                                                                                                                                                                                                                                                                                                                                                                                                                                                                                                                                                                                                                                                                                                                                                                                                                                                                                                                                                                                                                                                                                                                                                                                                                                                                                                                                                                                                                                                                                                                                                                                                                                                                                                                                                                                                                                                                                                                                                                                                                                                                                                                                                                                                                                                                                                                                                                                                                                                                                                                                                                                                                                                                                                                                                                                                                                                                                                                                                                                                                                                                                                                                                                                                                                                                                                                                                                                                                                                                                                                                                                                                                                                                                                                                                                                                                                                                                                                                                                                                                                                                                                                                                                                                                                                                                                                                                                                                                                                                                                                                                                                                                                                                                                                                                                                                                                                                                                                                                                                                                                                                                                                                                                                                                                                                                                                                                                                                                                                                                                                                                                                                                                                                                                                                                                                                                                                                                                                                                                                                                                                                                                                                                                                                                                                                                                                                                                                                                                                                                                                                                                                                                                                                                                                                                                                                                                                                                                                                                                                                                                                                                                                                                                                                                                                                                                                                                                                                                                                                                                                                                                                                                                                                                                                                                                
Consensus       MNRYTTMKQLGDGTYGSVLMGKSNESGELVAIKRMKRKFYSWDECMNLREVKSLKKLNHANVIKLKEVIRENDHLYFVFE

zMAK            MNRYTTLKQLGDGTYGSVLMGKSNESGELVAIKRMKRKFYSWEECMNLREVKSLKKLNHANVVKLKEVIRENDHLYFVFE
mMAK            MNRYTTMKQLGDGTYGSVLMGKSNESGELVAIKRMKRKFYSWDECMNLREVKSLKKLNHANVIKLKEVIRENDHLYFVFE
hMAK            MNRYTTMRQLGDGTYGSVLMGKSNESGELVAIKRMKRKFYSWDECMNLREVKSLKKLNHANVIKLKEVIRENDHLYFIFE
.....................................................................................................
                81                                                                                                                                                                                                                                                                                                                                                                                                                                                                                                                                                                                                                                                                                                                                                                                                                                                                                                                                                                                                                                                                                                                                                                                                                                                                                                                                                                                                                                                                                                                                                                                                                                                                                                                                                                                                                                                                                                                                                                                                                                                                                                                                                                                                                                                                                                                                                                                                                                                                                                                                                                                                                                                                                                                                                                                                                                                                                                                                                                                                                                                                                                                                                                                                                                                                                                                                                                                                                                                                                                                                                                                                                                                                                                                                                                                                                                                                                                                                                                                                                                                                                                                                                                                                                                                                                                                                                                                                                                                                                                                                                                                                                                                                                                                                                                                                                                                                                                                                                                                                                                                                                                                                                                                                                                                                                                                                                                                                                                                                                                                                                                                                                                                                                                                                                                                                                                                                                                                                                                                                                                                                                                                                                                                                                                                                                                                                                                                                                                                                                                                                                                                                                                                                                                                                                                                                                                                                                                                                                                                                                                                                                                                                                                                                                                                                                                                                                                                                                                
Consensus       YMKENLYQLMKDRENKLFPESVIRNIMYQILQGLAFIHKHGFFHRDMKPENLLCMGPELVKIADFGLARELRSQPPYTDY

zMAK            YMKENLYQLMKDRENKMFTENEIRNIMFQVLSGLAFVHKHGFFHRDMKPENLLCMGPELVKIADFGLAREIRSRPPYTDY
mMAK            YMKENLYQLMKDR-NKLFPESVIRNIMYQILQGLAFIHKHGFFHRDMKPENLLCMGPELVKIADFGLARELRSQPPYTDY
hMAK            YMKENLYQLMKDR-NKLFPESVIRNIMYQILQGLAFIHKHGFFHRDMKPENLLCMGPELVKIADFGLARELRSQPPYTDY
.....................................................................................................
                161                                                                                                                                                                                                                                                                                                                                                                                                                                                                                                                                                                                                                                                                                                                                                                                                                                                                                                                                                                                                                                                                                                                                                                                                                                                                                                                                                                                                                                                                                                                                                                                                                                                                                                                                                                                                                                                                                                                                                                                                                                                                                                                                                                                                                                                                                                                                                                                                                                                                                                                                                                                                                                                                                                                                                                                                                                                                                                                                                                                                                                                                                                                                                                                                                                                                                                                                                                                                                                                                                                                                                                                                                                                                                                                                                
Consensus       VSTRWYRAPEVLLRSSVYSSPIDVWAVGSIMAELYTLRPLFPGTSEVDEIFKICQVLGTPKKSDWPEGYQLASSMNFRFP

zMAK            VSTRWYRAPEVLLRSPVYSSPIDIWAVGCIMAELYTLRPLFPGNSEVDEIFKICQVLGTVKKSDWPEGHQLASAMNFRFP
mMAK            VSTRWYRAPEVLLRSSVYSSPIDVWAVGSIMAELYTFRPLFPGTSEVDEIFKICQVLGTPKKSDWPEGYQLASSMNFRFP
hMAK            VSTRWYRAPEVLLRSSVYSSPIDVWAVGSIMAELYMLRPLFPGTSEVDEIFKICQVLGTPKKSDWPEGYQLASSMNFRFP
.....................................................................................................
                241                                                                                                                                                                                                                                                                                                                                                                                                                                                                                                                                                                                                                                                                                                                                                                                                                                                                                                                                                                                                                                                                                                                                                                                                                                                                                                                                                                                                                                                                                                                                                                                                                                                                                                                                                                                                                                                                                                                                                                                                                                                                                                                                                                                                                                                                                                                                                                                                                                                                                                                                                                                                                                                                                                                                                                                                                                                                                                                                                                                                                                                                                                                                                                                                                                                                                                
Consensus       QCVPINLKTLIPNASNEAIQLMTEMLNWDPKKRPTASQALKHPYFQVGQVLGPSAHHLDSKQALHKQLQPLELKPSLQEV

zMAK            QCVPTPLKTLIPNAINEALDIMRDLLQWDPKKRPSAVKALRYPYFQVGQLLGPRPMTPDVRKAPVKAVLPSELRSEMQSV
mMAK            QCIPINLKTLIPNASSEAIQLMTEMLNWDPKKRPTASQALKHPYFQVGQVLGSSAHHLDTKQTLHKQLQPLEPKPSSSER
hMAK            QCVPINLKTLIPNASNEAIQLMTEMLNWDPKKRPTASQALKHPYFQVGQVLGPSSNHLESKQSLNKQLQPLESKPSLVEV
.....................................................................................................
                321                                                                                                                                                                                                                                                                                                                                                                                                                                                                                                                                                                                                                                                                                                                                                                                                                                                                                                                                                                                                                                                                                                                                                                                                                                                                                                                                                                                                                                                                                                                                                                                                                                                                                                                                                                                                                                                                                                                                                                                                                                                                                                                                                                                                                                                                                                                                                                                                                                                                                                                                                                                                                                                                                                                                                                                                                                                                                                                                                                                                                                                                                                                                                                                                                                                                                
Consensus       DPKPLPDIIDQPAGQPQPKNSHQPLQPIQPPQNLSQHDPPKQQGHEKPPQTLFPSIIKKIPGGENSTLGHKGGRRRWGQT

zMAK            SE---PVLPSQ--TKGQSRNSHQPLQQIPLPQSLTQTDTVA-------------LHTQKVVGGENSLMGLKNGRRRWGQT
mMAK            DPKPLPNILDQPAGQPQPKQGHQPLQTIQPPQNTVTHPPPKQQGHQKPPQTMFPSIIKTIPVNSVSTLGHKGARRRWGQT
hMAK            EPKPLPDIIDQVVGQPQPKTSQQPLQPIQPPQNLSVQQPPKQQSQEKPPQTLFPSIVKNMPTKPNGTLSHKSGRRRWGQT
.....................................................................................................
                401                                                                                                                                                                                                                                                                                                                                                                                                                                                                                                                                                                                                                                                                                                                                                                                                                                                                                                                                                                                                                                                                                                                                                                                                                                                                                                                                                                                                                                                                                                                                                                                                                                                                                                                                                                                                                                                                                                                                                                                                                                                                                                                                                                                                                                                                                                                                                                                                                                                                                                                                                                                                                                                                                                                                                                                                                                                                                                                                                                                                                                                                
Consensus       IFKSGDSWDDIEDSDFGASHSKKPSMGACKEKRKKDSPFRFPDPGFSGSNHFKGENKKLPATSRSLKSDSELSTASTAKQ

zMAK            NMKPSDSWDDSDCSDTAASLSKKPSKGPEEEKTTPQPKEQKPLYTFST-------VTKLPNTSRLNQSDSSHQSTSSARQ
mMAK            VFKSGDSCDDIED-DLGASHSKKPSMEACKEK-KKESPFRFPDSGLPVSNHFKGENRNLHA-SVSLKSDPNLSTASTAKQ
hMAK            IFKSGDSWEELEDYDFGASHSKKPSMGVFKEKRKKDSPFRLPEPVPSGSNHSTGENKSLPA-VTSLKSDSELSTAPTSKQ
.....................................................................................................
                481                                                                                                                                                                                                                                                                                                                                                                                                                                                                                                                                                                                                                                                                                                                                                                                                                                                                                                                                                                                                                                                                                                                                                                                                                                                                                                                                                                                                                                                                                                                                                                                                                                                                                                                                                                                                                                                                                                                                                                                                                                                                                                                                                                                                                                                                                                                                                                                                                                                                                                                                                                                                                                                                                                                                                                                                                                                                                                                                                                                                                                                                
Consensus       YYLKQSRYLPGVNPKNVSLIASGKEINPHFWDNSQLFPKSLGPIGAALAFKRSNAEDSIIKPIEKLSCNEKFAEKLEDPQ

zMAK            HYLRQSRYMPGLISKNTQSLSSK-ESQQDFWDTSALMSKPLAPIGGAPMS---------------------------RISP
mMAK            YYLKQSRYLPGVNPKNVSLVAGGKDINSHSWNN-QLFPKSLGSMGADLSFKRSNAEDSIIKPIENLSCTGKSAEQLEDPQ
hMAK            YYLKQSRYLPGVNPKKVSLIASGKEINPHTWSN-QLFPKSLGPVGAELAFKRSNAEESIIKPIEKLSCNETFPEKLEDPQ
.....................................................................................................
                561                                                                                                                                                                                                                                                                                                                                                                                                                                                                                                                                                                                                                                                                                                                                                                                                                                                                                                                                                                                                                                                                                                                                                                                                                                                                                                                                                                                                                                                                                                                                                                                                                                                                                                                                                                                                                                                                                                                                                                                                                                                                                                                                                                                                                                                                                                                                                                                                                                                                                                                                                                                                                                                                                                                                                                                                                                                                                                                                                                                                                                                                
Consensus       GNLGSYTTYNQGGYIPSFLKKEVGSAGQRIQLAPLGAQASLDLSATADCKTGKAKPSKSKPSSTVSVNDNSEDDYTWKTK

zMAK            GNFVTTTYNLSGGYIPSFQKKEVGSVGQRIQLAPLGHQHALDLSATADCKTGKAKPSKSKPSSTVSVNDNSEDYDGWKRR
mMAK            GNLGSYTTYNQTGYMPSFLKKEVGSAGQRIQLAPLGASAS---------------------------------DYTWSTK
hMAK            GNLGSYATYNQSGYIPSFLKKEVQSAGQRIHLAPLNAIAS---------------------------------EYTWNTK
.....................................................................................................
                641                                                                                                                                                                                                                                                                                                                                                                                                                                                                                                                                                                                                                                                                                                                                                                                                                                                                                                                                                                                                                                                                                                                                                                                                                                                                                                                                                                                                                                                                                                                                                                                                                                                                                                                                                                                                                                                                                                                                                                                                                                                                                                                                                                                                                                                                                                                                                                                                                                                                                                                                                                                                                                                                                                                                                                                                                                                                                                                                                                                                                                                                
Consensus       TGRGQFSGRTYNPTAKNSLNIVNRAQPVPSVHGRTDWVAKYGGHR

zMAK            AERTQLKGTSYSALGKNSANLITHAPSVQPVHGRIDWAAKYGSHR
mMAK            TGRGQFSGRTYNPTAKN-LNIVNRTQPVPSVHGRTDWVAKYGGHR
hMAK            TGRGQFSGRTYNPTAKN-LNIVNRAQPIPSVHGRTDWVAKYGGHR
```

Amino acid sequence identity percentage

	Full length	Kinase domain	C'-terminus
zMAK vs mMAK	50% (323/646)	86.17% (243/282)	21.82% (79/362)
zMAK vs hMAK	51.38% (333/648)	88.65% (250/282)	21.97% (80/364)
mMAK vs hMAK	83.64% (542/648)	97.86% (275/281)	72.52% (264/364)
Among the three animals	47.22% (306/648)	85.10% (240/282)	17.03% (62/364)

Figure S4

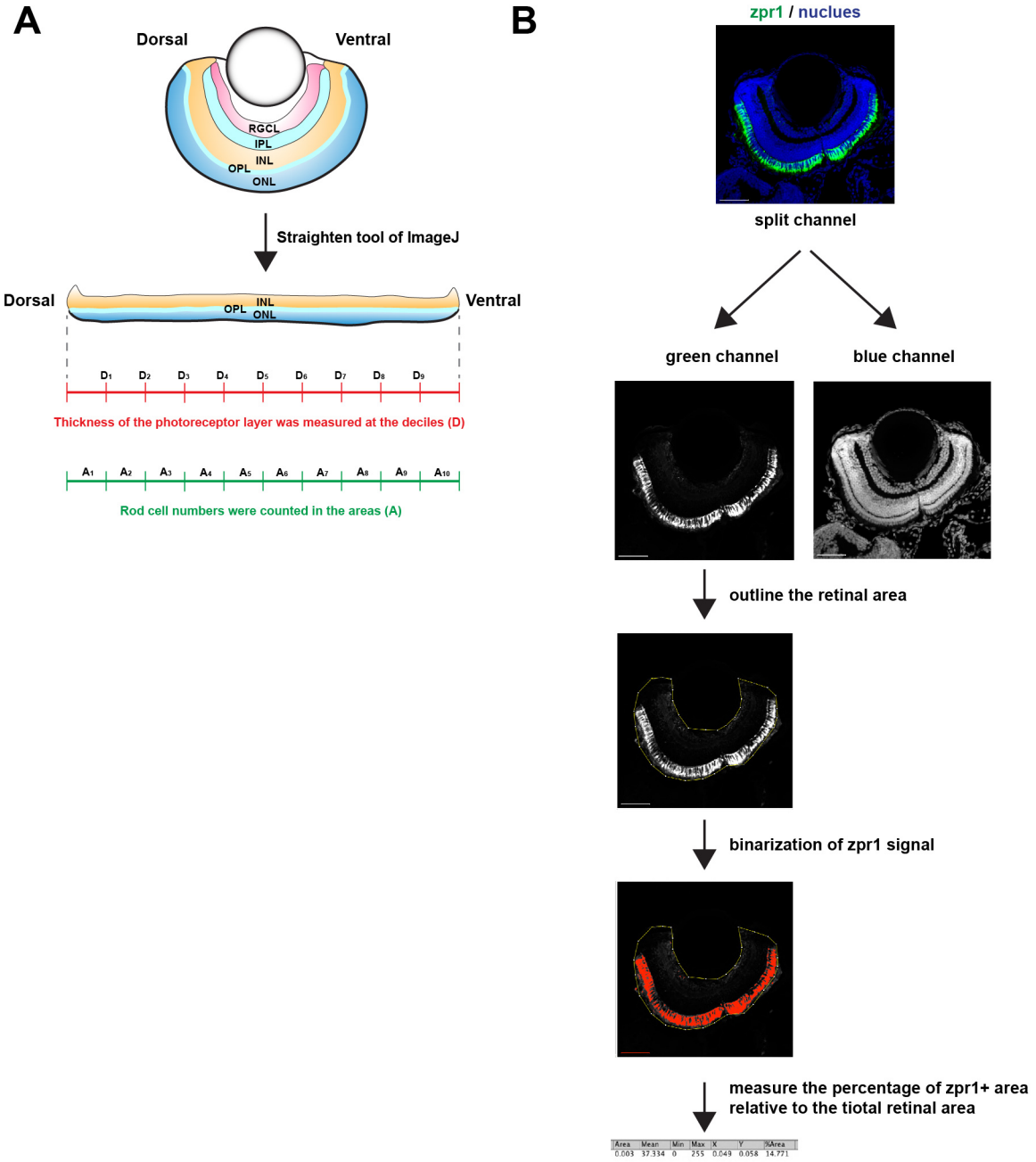
A
Dorsal
Ventral
RGCL
IPL
INL
OPL
ONL
Straighten tool of ImageJ
Dorsal
Ventral
INL
OPL
ONL
D1 D2 D3 D4 D5 D6 D7 D8 D9
Thickness of the photoreceptor layer was measured at the deciles (D)
A1 A2 A3 A4 A5 A6 A7 A8 A9 A10
Rod cell numbers were counted in the areas (A)
B
zpr1 / nuclues
split channel
green channel
blue channel
outline the retinal area
binarization of zpr1 signal
measure the percentage of zpr1+ area
relative to the tiotal retinal area
Area Mean Min Max X Y %Area
0.003 37.334 0 255 0.049 0.058 14.771

Figure S5